SUPPLEMENTARY MATERIAL

Coordinated conformational changes in P450 decarboxylases enable hydrocarbons production from renewable feedstocks

Wesley Cardoso Generoso[1], Alana Helen Santana Alvarenga[1], Isabelle Taira Simões[1], Renan Yuji Miyamoto[1], Ricardo Rodrigues de Melo[1], Ederson Paulo Xavier Guilherme[1], Fernanda Mandelli[1], Clelton Aparecido Santos[1], Rafaela Prata[1], Camila Ramos dos Santos[1], Felippe Mariano Colombari[1], Mariana Abrahão Bueno Morais[1], Rodrigo Fernandes[2], Gabriela Felix Persinoti[1], Mario Tyago Murakami[1], Leticia Maria Zanphorlin[1*]

[1]Brazilian Biorenewables National Laboratory, Brazilian Center for Research in Energy and Materials, Campinas, SP, Brazil.

[2]Sinochem Petróleo Brasil LTDA, Rio de Janeiro, RJ, Brazil.

*Corresponding author: leticia.zanphorlin@lnbr.cnpem.br

This PDF file includes:

Supplementary Figures 1 to 30

Supplementary Tables 1 to 9

Supplementary Methods

Supplementary References

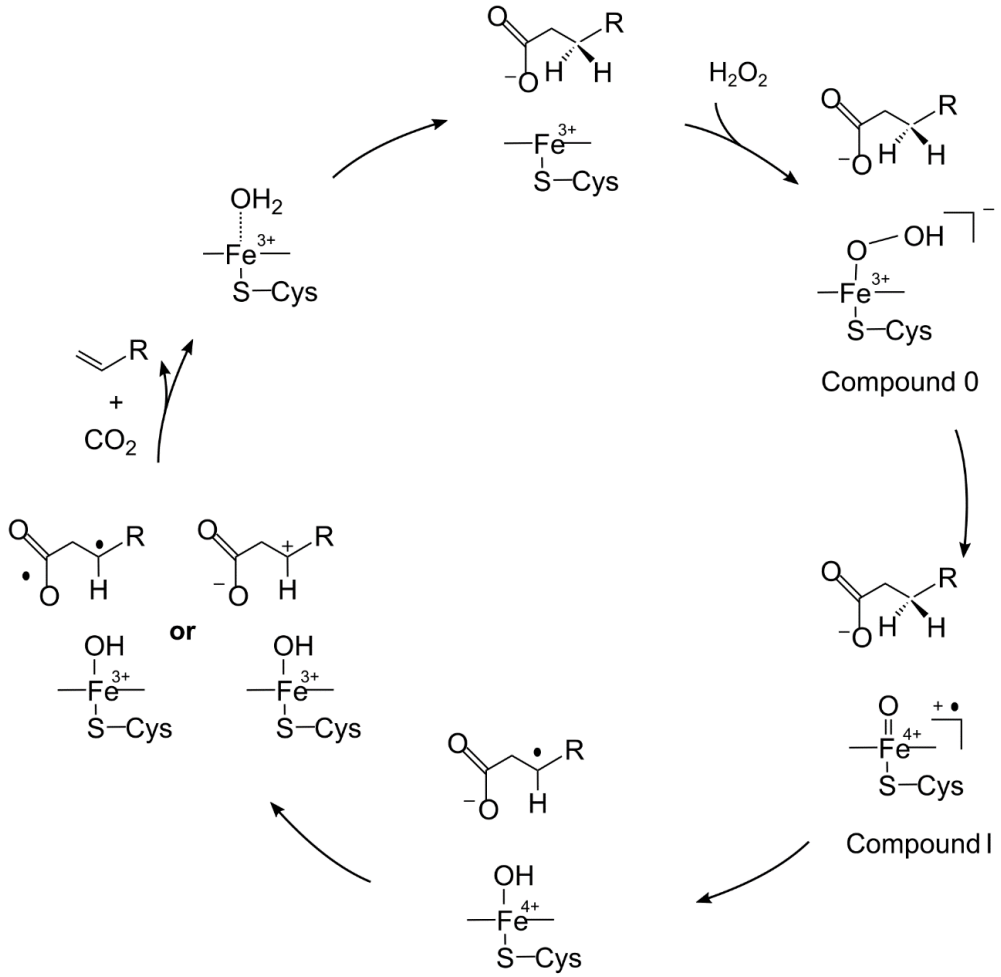

Supplementary Figure 1. Simplified P450 catalytic cycle of fatty acid decarboxylases employing the peroxide shunt as sole iron activation. In sake of clarity, heme group is present as a ferric ion (Fe^{3+}) coordinated by the cysteine thiolate (S). Despite CYP152 capability to perform substrate hydroxylation, this reaction is not contemplated in this scheme.

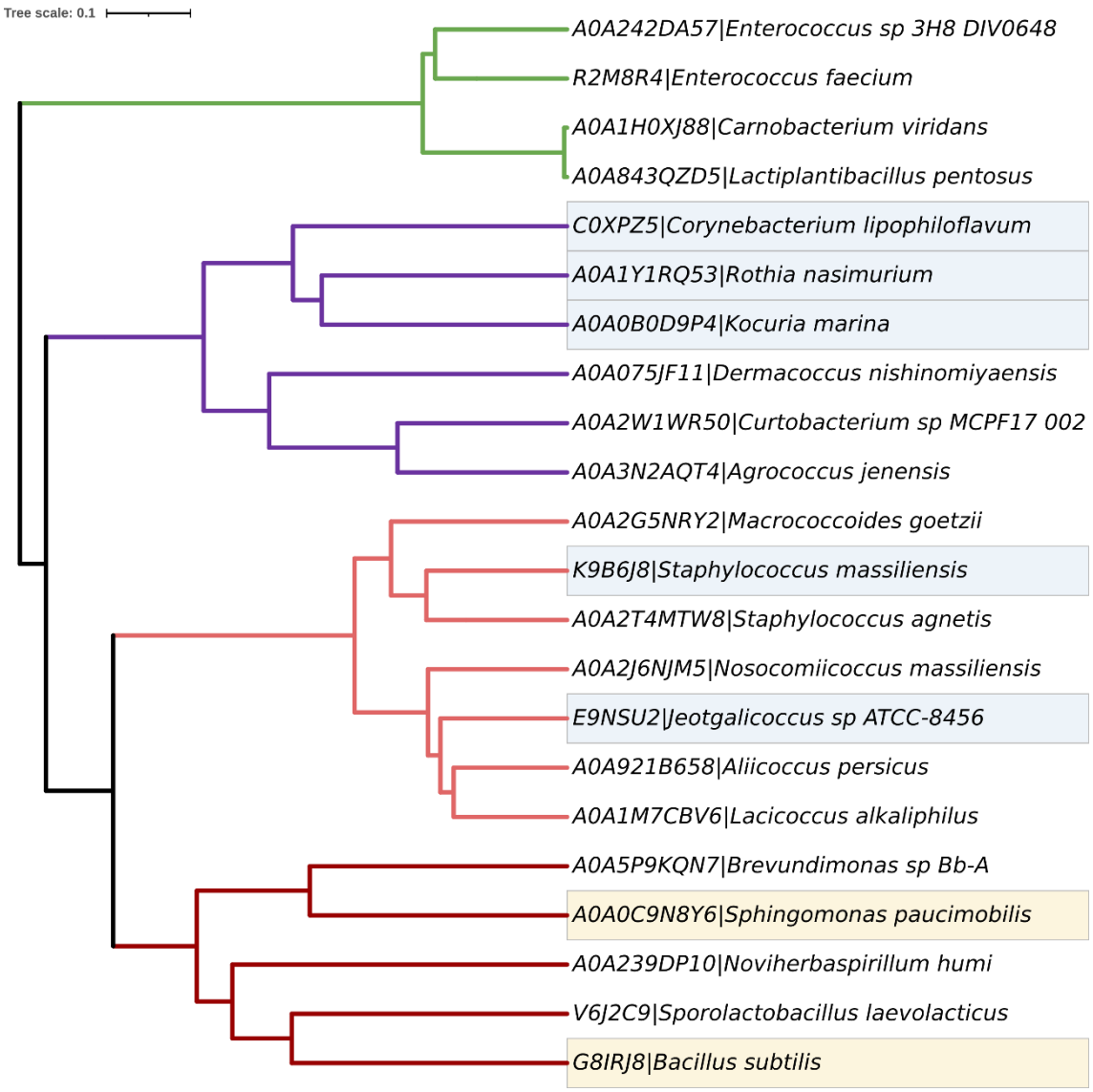

Supplementary Figure 2. Phylogenetic tree of CYP152 members obtained from SSN analysis. Branch colors correlate with SSN Clusters: I, red; II, purple; III, pink; IV, green. Nodes highlighted in blue comply decarboxylases [$OleTP_{CL}$, $OleTP_{RN}$, $OleT_{KM}$, $OleT_{SM}$, and $OleT_{JE}$] and in yellow comply already characterized hydroxylases [$P450_{SP\alpha}$ and $P450_{BS\beta}$]. Uniprot ID initiates node identification, followed by species name.

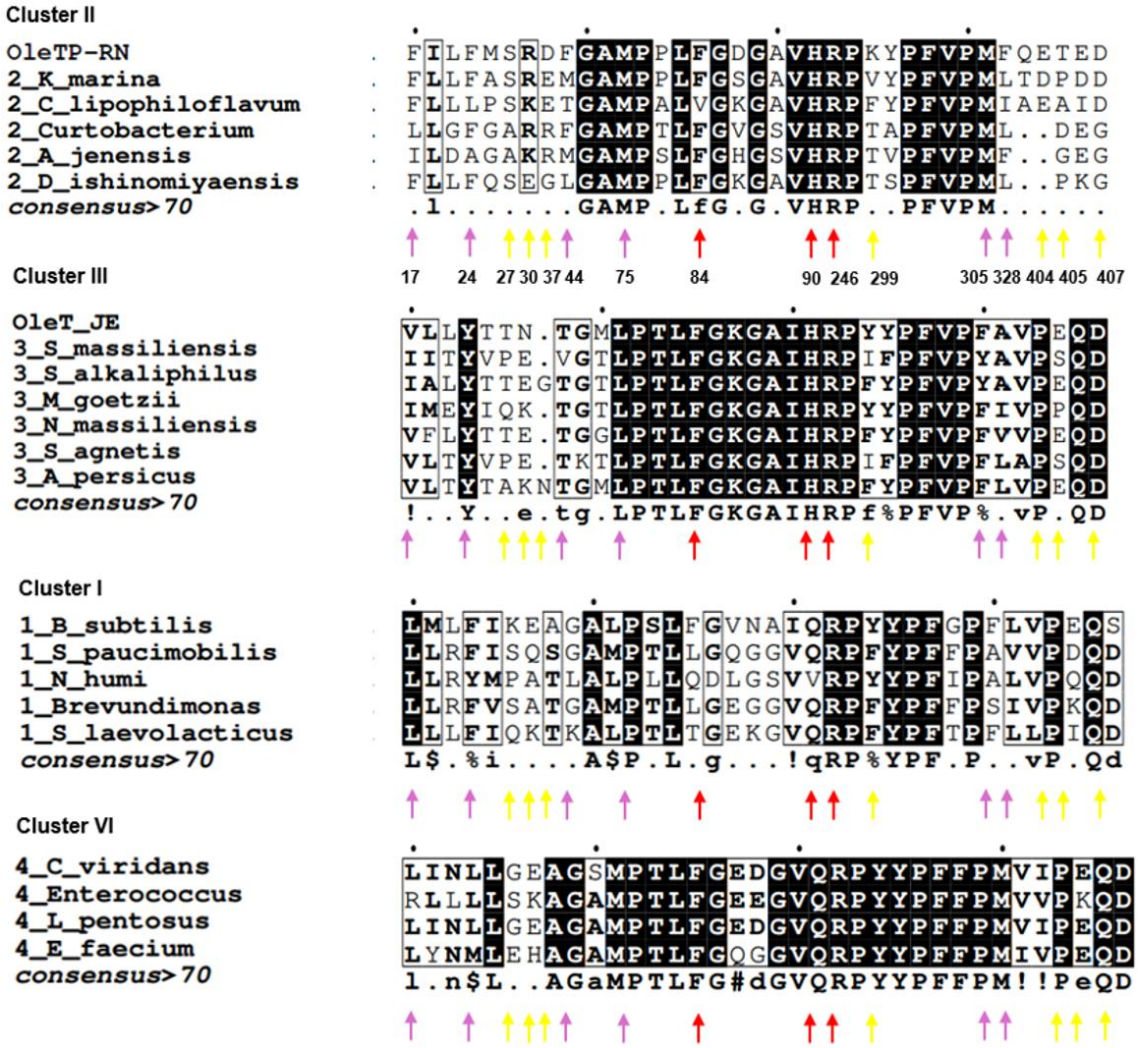

Supplementary Figure 3. Multiple sequence alignment of representative sequences highlighting the sequence conservation intra-cluster on key regions encompassing the hydrophobic cradle (pink arrows), dimeric interface (yellow), and catalytic residues (red arrows). Residue numbers refer to the $OleTP_{RN}$ sequence.

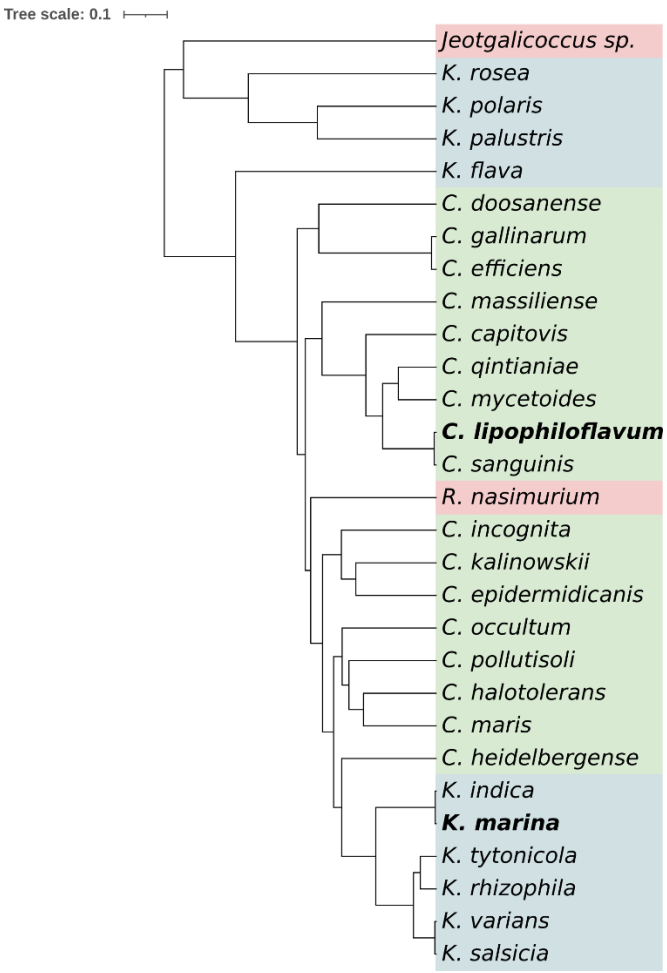

Supplementary Figure 4. Phylogenetic tree of putative CYP152 decarboxylases obtained from BLAST analysis. Nodes highlighted in blue represent *Corynebacterium* species and in green represent *Kocuria* species. *Jeotgaliccocus* sp. and *Rothia nasimurium* references branches are indicated in blue and red, respectively.

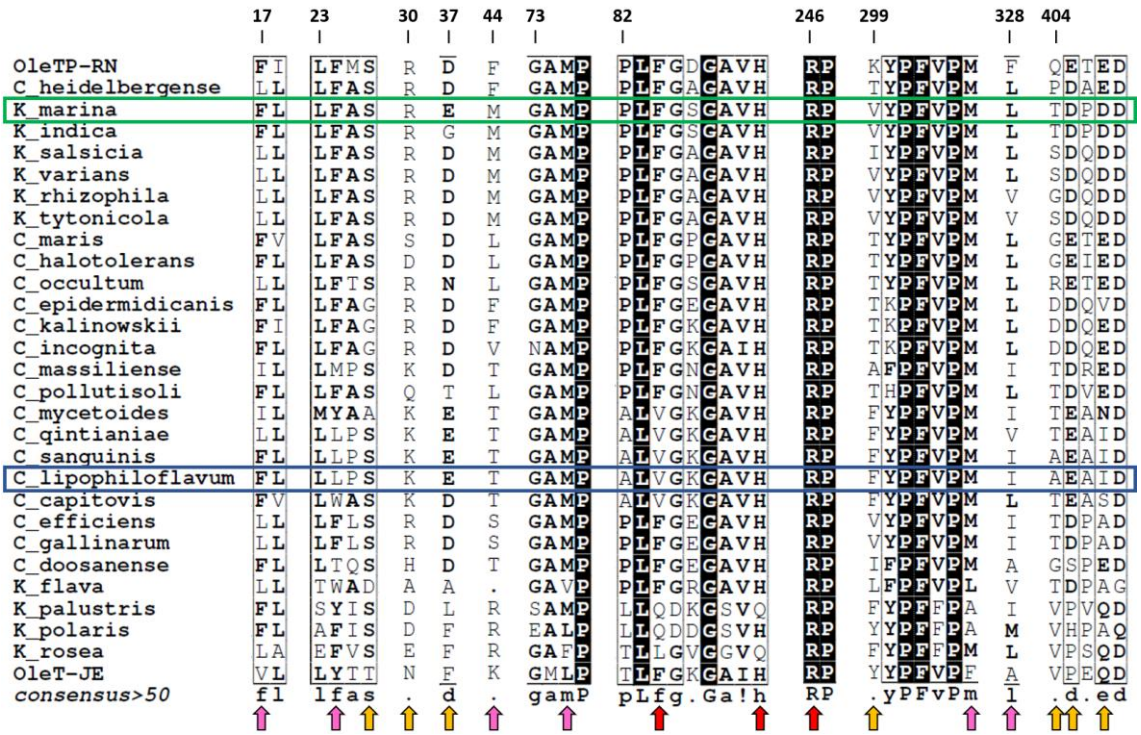

Supplementary Figure 5. The multiple sequence alignment of putative CYP152 members of *Corynebacterium* and *Kocuria* species. Sequence alignment was performed with Multalin (http://multalin.toulouse.inra.fr/) and represented with ESPrint 3.0 (https://espript.ibcp.fr/ESPript/ESPript/). Red arrows indicate the catalytic site-forming amino acids, pink arrows indicate the hydrophobic cradle, and yellow arrows indicate the dimeric interface.

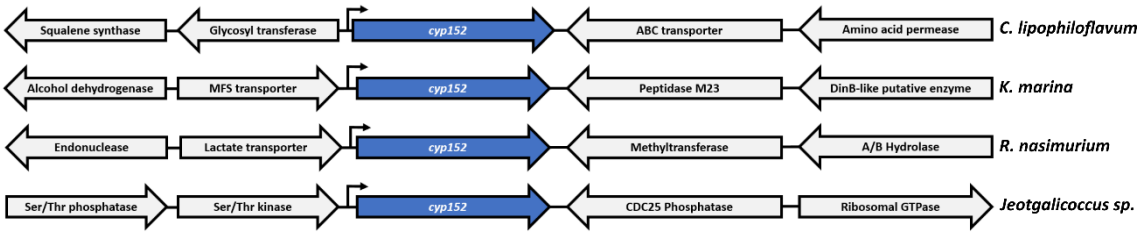

Supplementary Figure 6. Genomic context of CYP152 members in *C. lipophiloflavum*, *K. marina*, *R. nasimurum*, and *Jeotgalicoccus sp.*

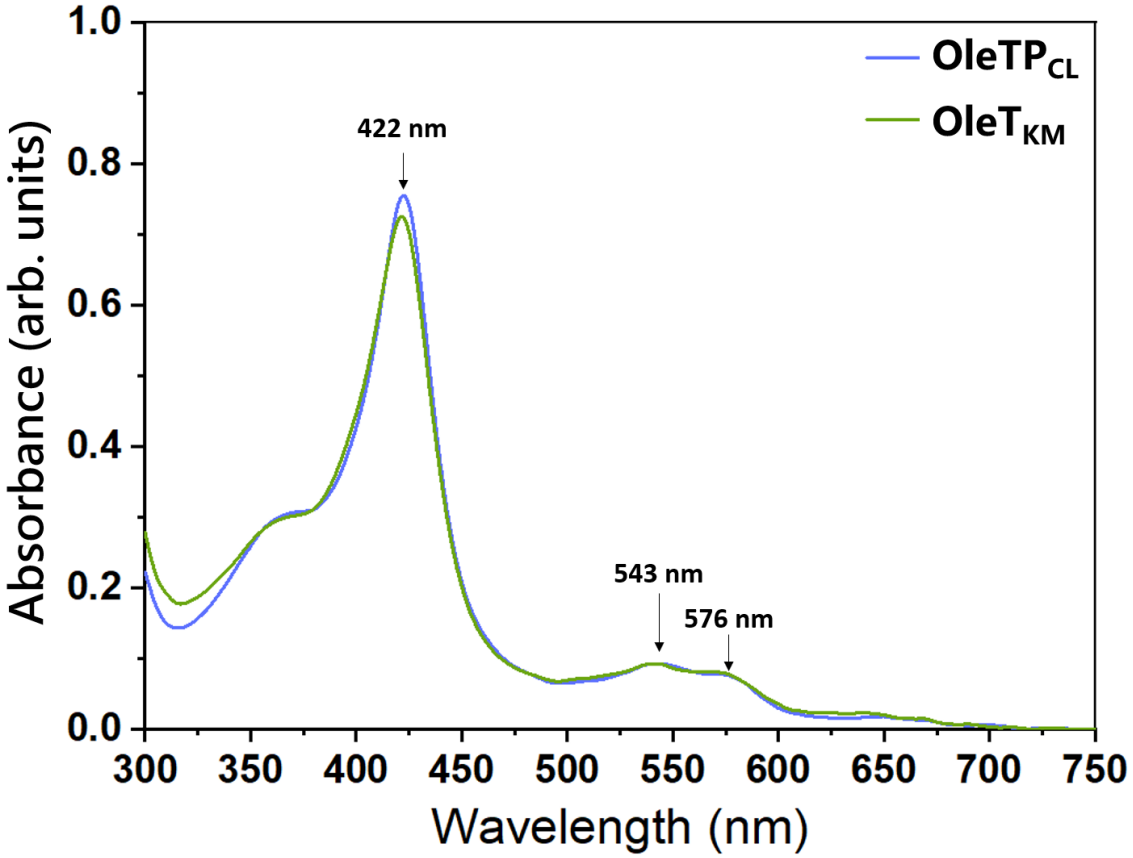

Supplementary Figure 7. OleT$_{KM}$ and OleTP$_{CL}$ UV-visible spectrum, *i.e.* Soret peak around 420 nm and Q-bands at 540 and 575 nm in the low spin ferric resting state.

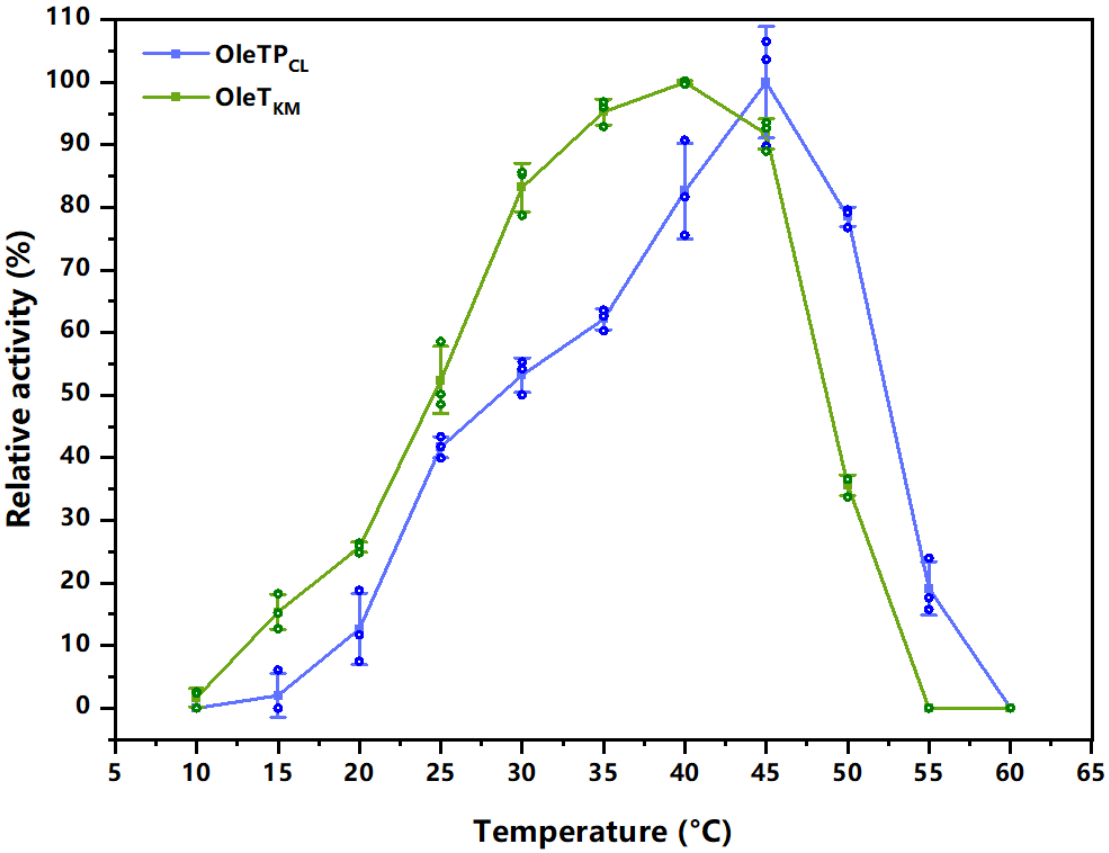

Supplementary Figure 8. Effects of temperature on the relative activity of OleTP$_{CL}$ and OleT$_{KM}$. Experiments were conducted in 100 mM sodium phosphate buffer (pH 7.5) with 200 µM palmitic acid, 0.5 µM enzyme, and 100 µM H_2O_2 for 10 min varying reaction temperatures. The remaining H_2O_2 was measured by the ferrous oxidation - xylenol orange (FOX) assay. Results are expressed as mean ± SD from three independent experiments (n = 3).

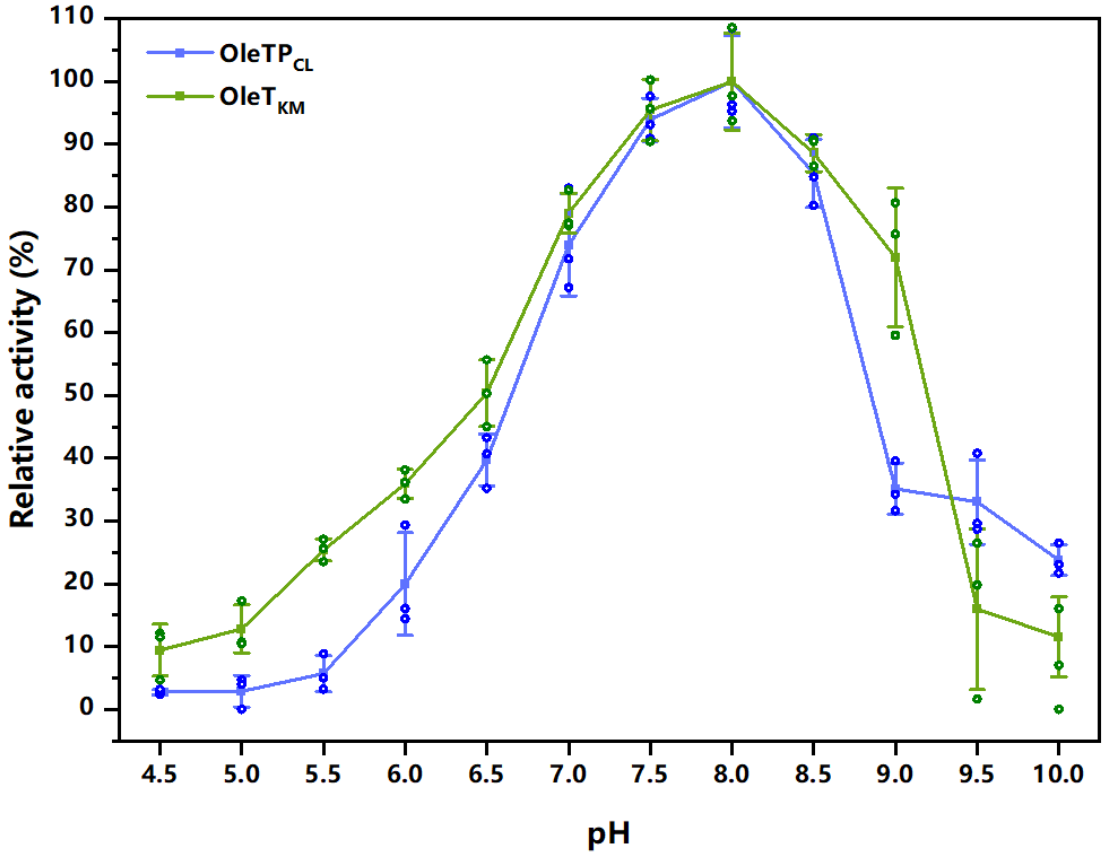

Supplementary Figure 9. Effects of pH on the relative activity of $OleTP_{CL}$ and $OleT_{KM}$. Experiments were conducted with 200 µM palmitic acid, 0.5 µM enzyme, and 100 µM H_2O_2 for 10 min varying reaction buffer. The best-defined temperature was employed for pH screening. The remaining H_2O_2 was measured by the ferrous oxidation−xylenol orange (FOX) assay. Results are expressed as mean ± SD from three independent experiments (n=3). For the pH profile, reactions were performed with 100 mM of each of the following buffers: sodium-citrate (pH 4.0, 4.5, 5.0, and 5.5), sodium phosphate (pH 6.0, 6.5, 7.0, and 8.0), Tris–HCl (pH 9.0), and glycine (pH 10.0). Results are expressed as mean ± SD from three independent experiments (n = 3).

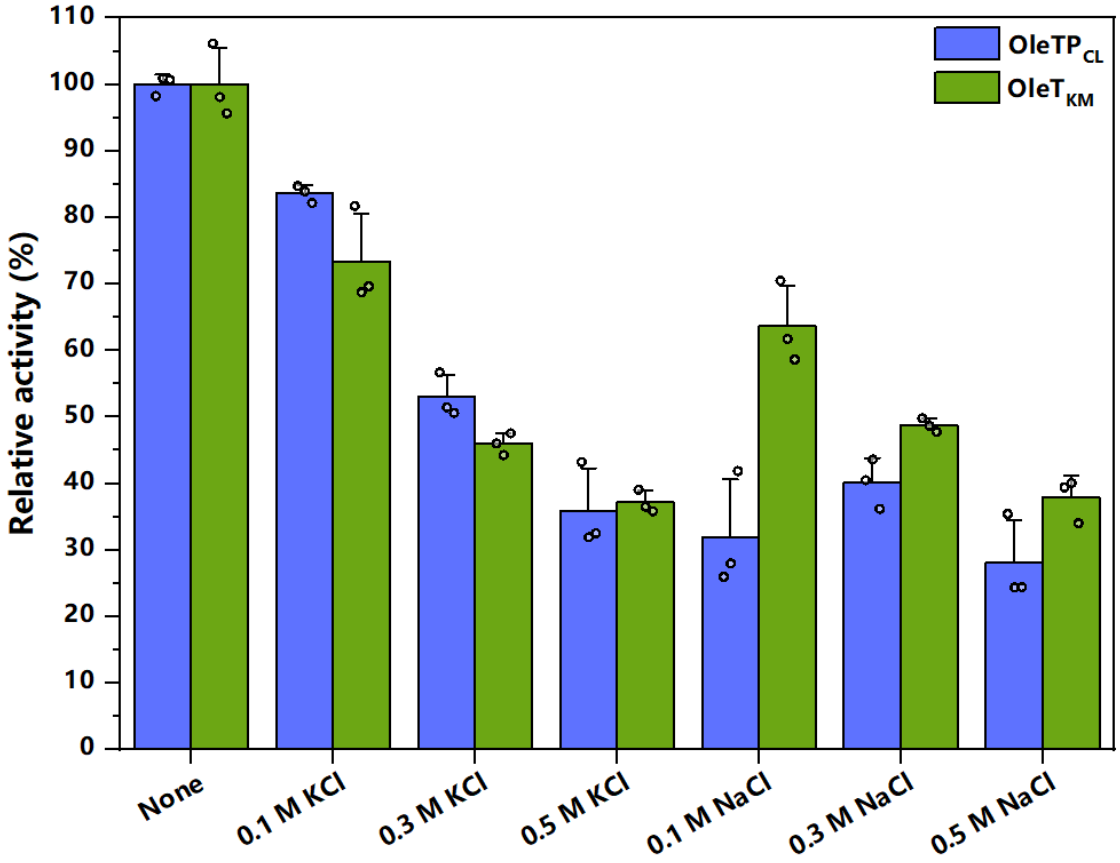

Supplementary Figure 10. Salt dependence on the relative activity of $OleTP_{CL}$ and $OleT_{KM}$. Experiments were conducted with 200 μM palmitic acid, 0.5 μM enzyme, and 100 μM H_2O_2 for 10 min, varying NaCl and KCl concentrations in the reaction buffer. The best-defined condition for temperature and pH was employed for salt screening. The remaining H_2O_2 was measured by the ferrous oxidation-xylenol orange (FOX) assay. Results are expressed as mean ± SD from three independent experiments (n = 3).

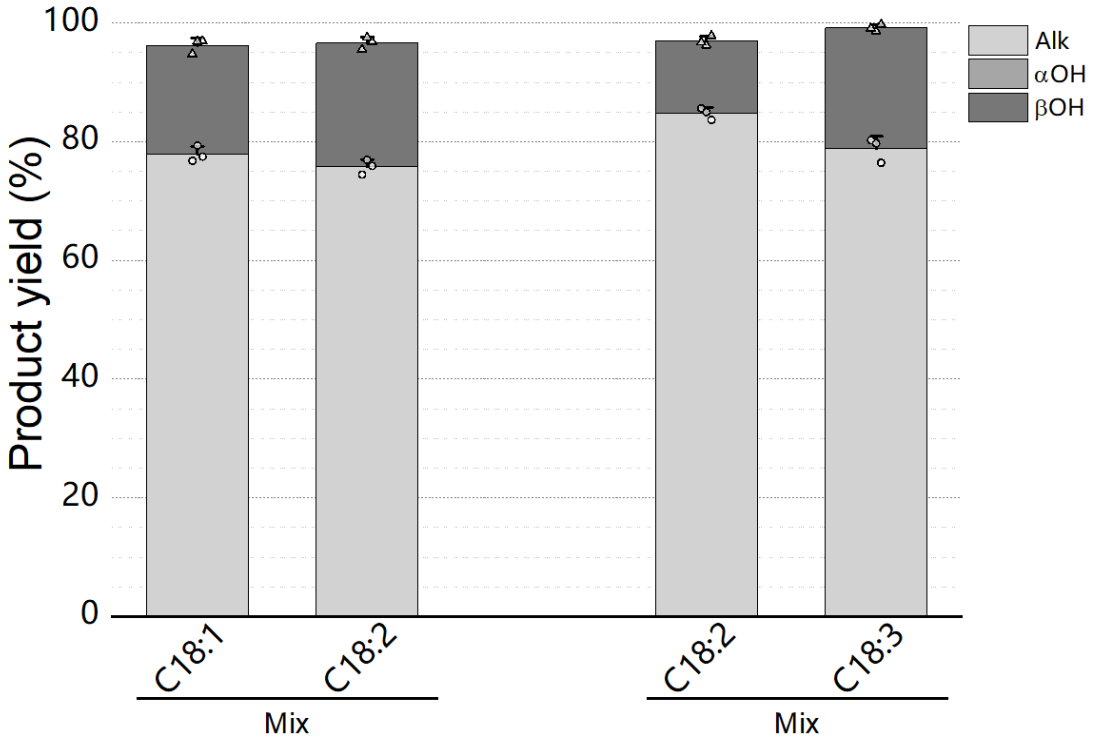

Supplementary Figure 11. The product yield of turnover reactions of $OleTP_{CL}$ with different unsaturated FA substrate combinations. The lighter, medium, and darker bar colors represent alkene, α-hydroxy fatty acid, and β-hydroxy fatty acid, respectively. Experimental conditions: 2 μM enzyme, 500 μM total substrate, 600 μM H_2O_2, at 45°C in 100 mM sodium phosphate buffer (pH 7.5) for 1 h. Results are expressed as mean ± SD from three independent experiments (n = 3).

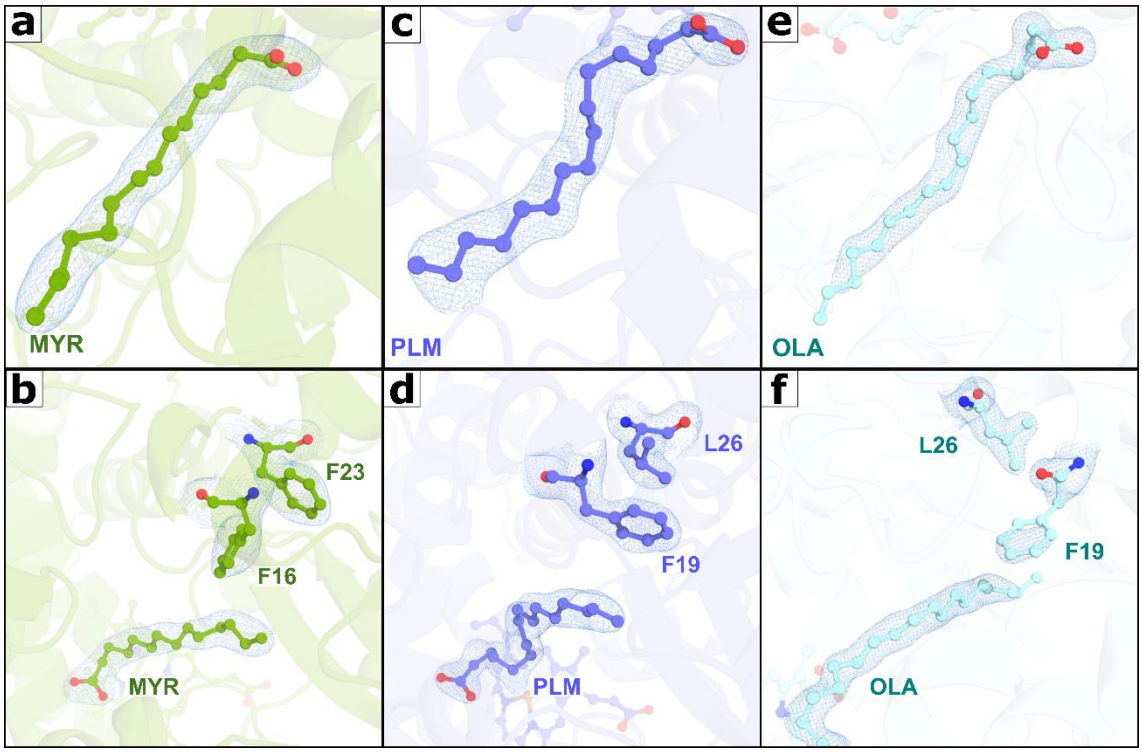

Supplementary Figure 12. Electron density map of $OleT_{KM}$ active site accommodating a myristate **(a, b)**, and $OleTP_{CL}$ active site with palmitate **(c, d)** and oleate substrates **(e, f)**. The composite omit mFo-dFc maps highlight the substrate density fit **(a, c, e)** and the amino acids engaged in the flexibility or stiffening of the distal phenylalanine **(b, d, f)**. All maps are shown in navy blue and contoured at 1.0 σ.

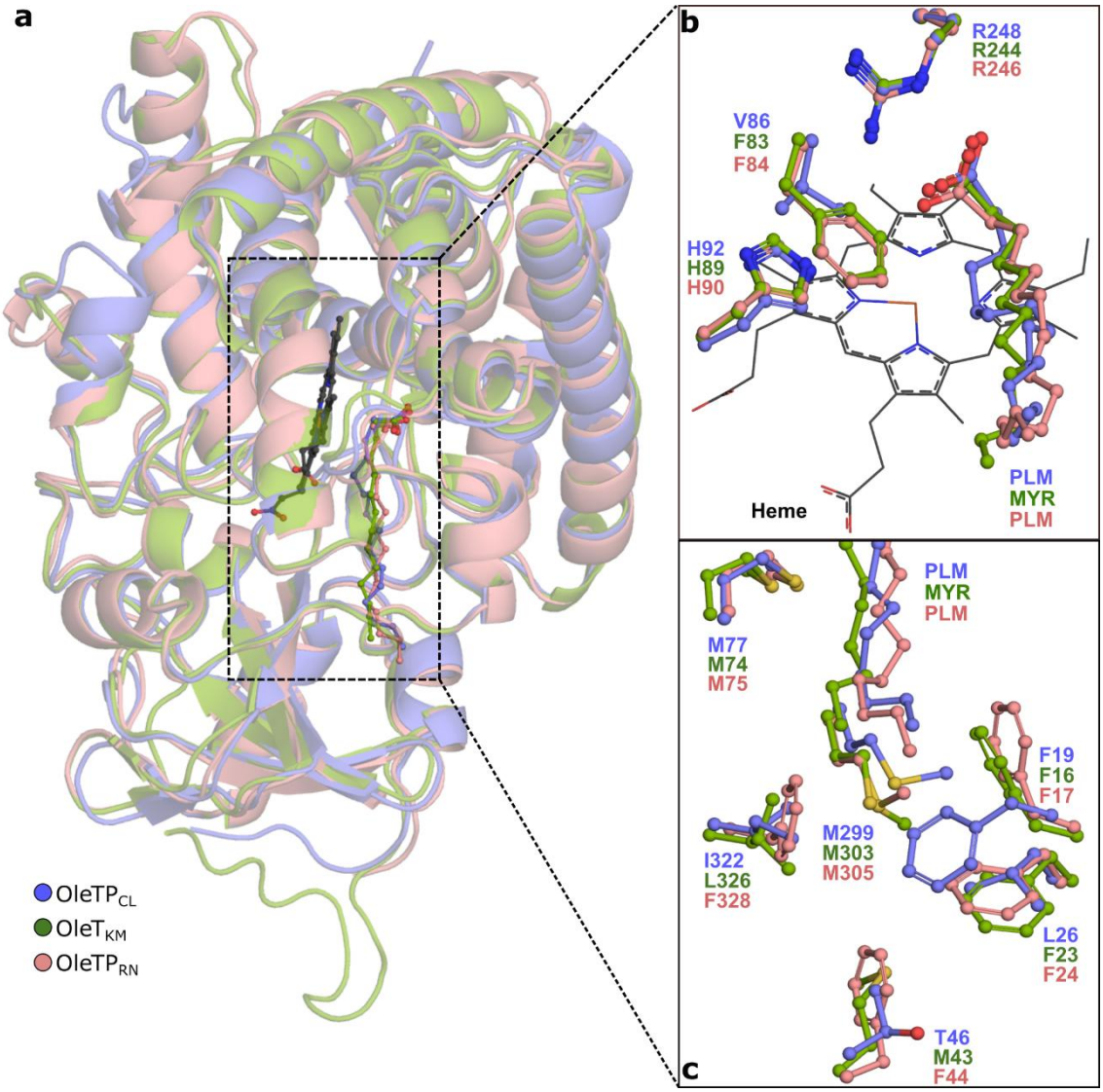

Supplementary Figure 13. (a) Cartoon representation of superimposed OleTP$_{CL}$, OleT$_{KM}$, and OleTP$_{RN}$, showing substrates and overall topology conservation. **(b)** Catalytic site showing canonical amino acid positioning relative to the heme group. **(c)** View of amino acids responsible for the hydrophobic cradle motif important for substrate positioning.

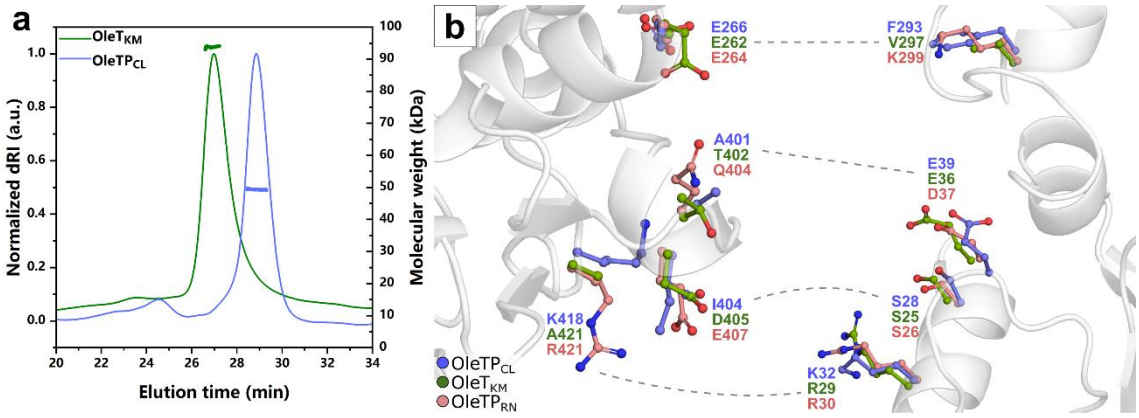

Supplementary Figure 14. (a) Multi-angle light scattering coupled with size exclusion chromatography (SEC-MALS) analysis of $OleTP_{CL}$ and $OleT_{KM}$, indicating a prevalent monomeric form for $OleTP_{CL}$, while $OleT_{KM}$ is also observed as a dimer in solution. **(b)** Cartoon representation of hypothetical protein dimerizations, highlighting amino acids involved in the dimer interface of $OleTP_{RN}$. Dashed lines represent amino acid interactions based on the $OleTP_{RN}$ dimerization pattern.

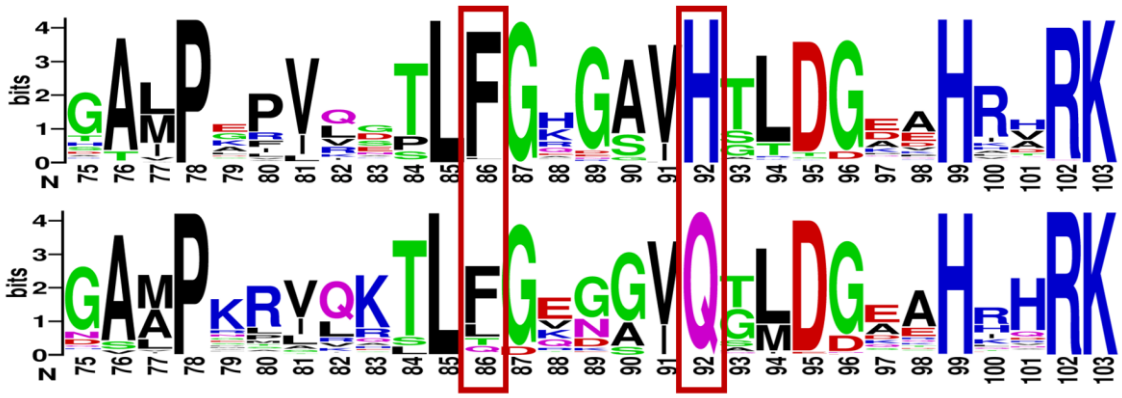

Supplementary Figure 15. Amino acid conservation of CYP152 members retrieved from SSN analysis that possess either a histidine or a glutamine at the catalytic site. The alignment representation was created with Weblogo (https://weblogo.berkeley.edu/logo.cgi), and numbering refers to OleTP$_{CL}$ amino acid sequence. Red squares highlight the canonical histidine and phenylalanine at the catalytic site of CYP152 decarboxylases. Statistical frequency is automatically generated by the online application, therefore, no numerical representation is included in the source data file.

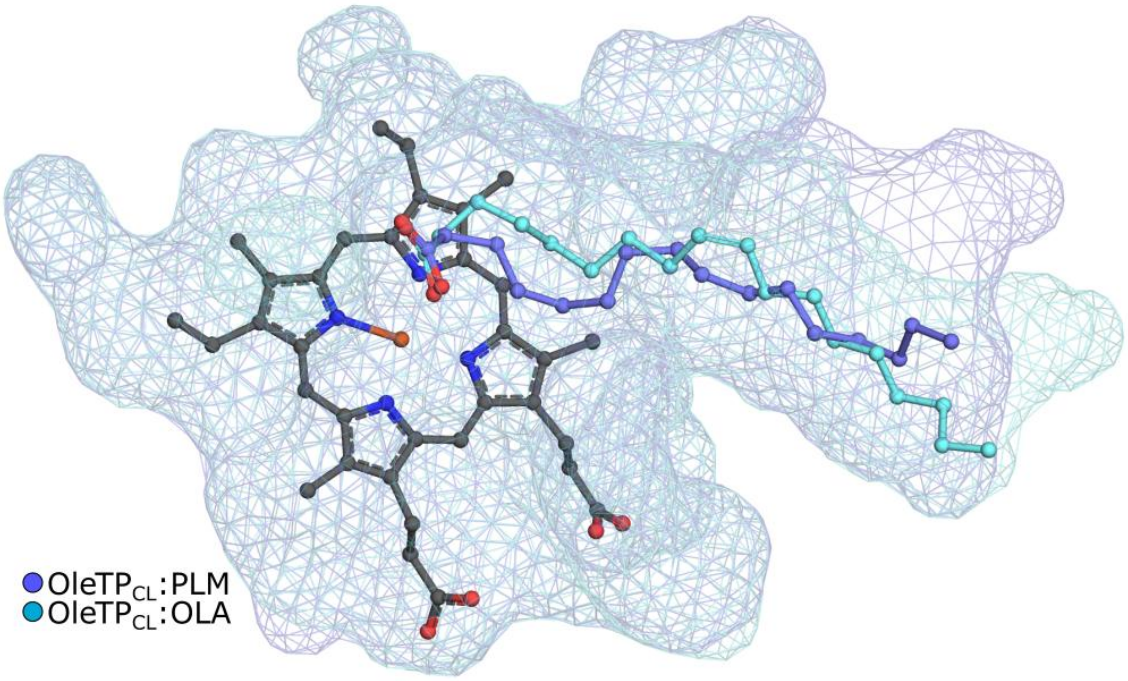

Supplementary Figure 16. Comparison of binding pocket conformation of OleTP$_{CL}$ complexed with either palmitic acid or oleic acid. The protein internal surfaces are represented as wire to improve visualization of both binding pockets.

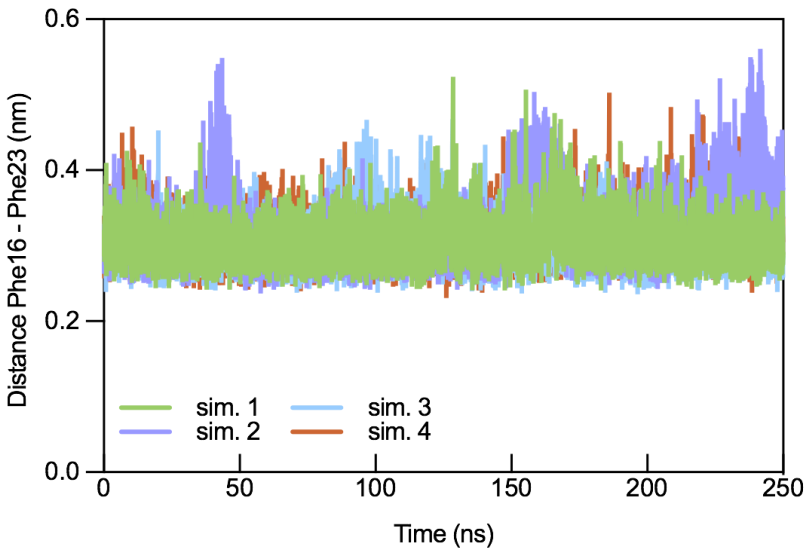

Supplementary Figure 17. Distance between the atoms F16 HA and F23 CG during 250 ns of production from $OleT_{KM}$ four independent molecular dynamics simulations.

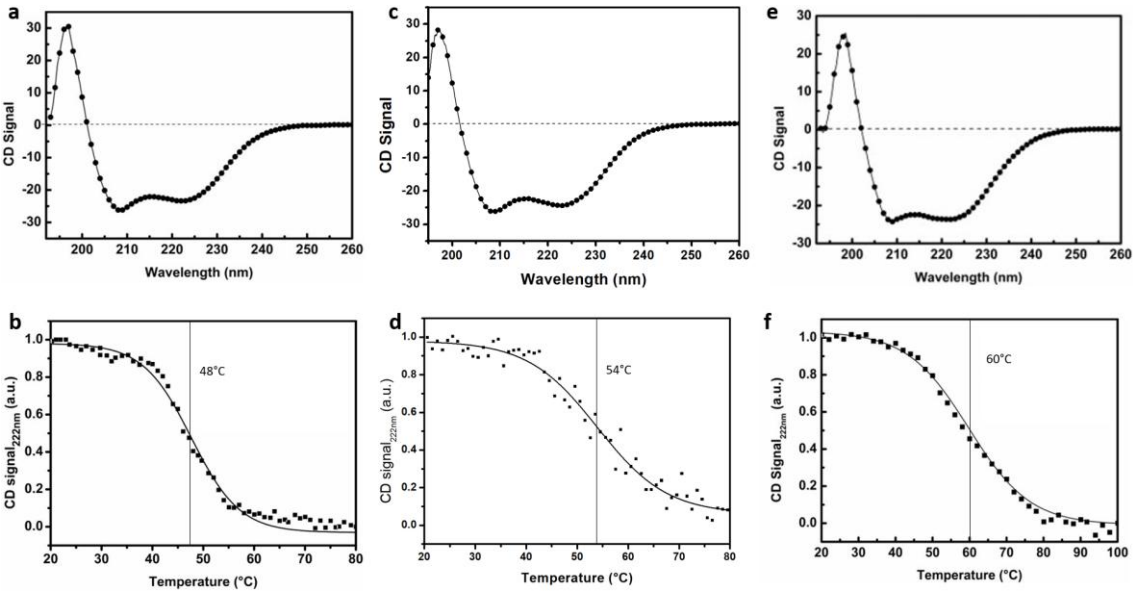

Supplementary Figure 18. Circular dichroism (CD) ellipticity analysis of $OleTP_{CL}$ **(a)**, $OleTP_{CL}$-L26F **(c),** and $OleT_{KM}$ **(e)** over a wavelength range of 190 - 260 nm at 20°C. The thermal unfolding profile, following ellipticity at 222 nm of $OleTP_{CL}$ **(b)**, $OleTP_{CL}$-L26F **(d)** and $OleT_{KM}$ **(f)**. The buffer employed in the experiments was 100 mM sodium phosphate at pH 7.5 with 150 mM NaCl and 5 % w/v glycerol.

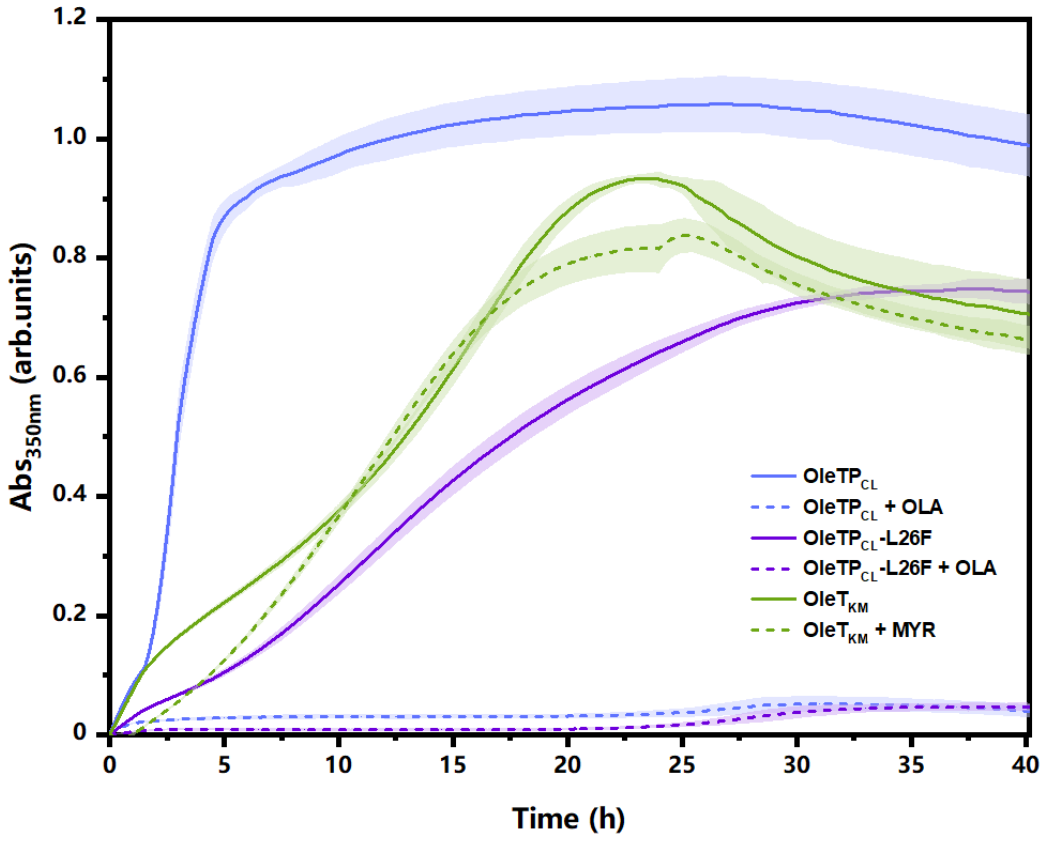

Supplementary Figure 19. Enzyme thermal resistance analysis at 42°C of $OleTP_{CL}$, $OleTP_{CL}$-L26F, and $OleT_{KM}$ in the presence and absence of substrate. Changes in the absorbance at 350 nm correspond to the free heme group released in the solution. A 100-µL enzyme solution (10 µM) was incubated in 384-well plates under controlled humidifying conditions to avoid evaporation. The buffer employed was the same as the one used for purification [30 mM phosphate buffer, 300 mM NaCl, 5% glycerol, pH 7.5]. Concomitantly, the enzymes were incubated with 500 µM substrate (traced lines). The experiment was conducted in quadruplicate for each condition.

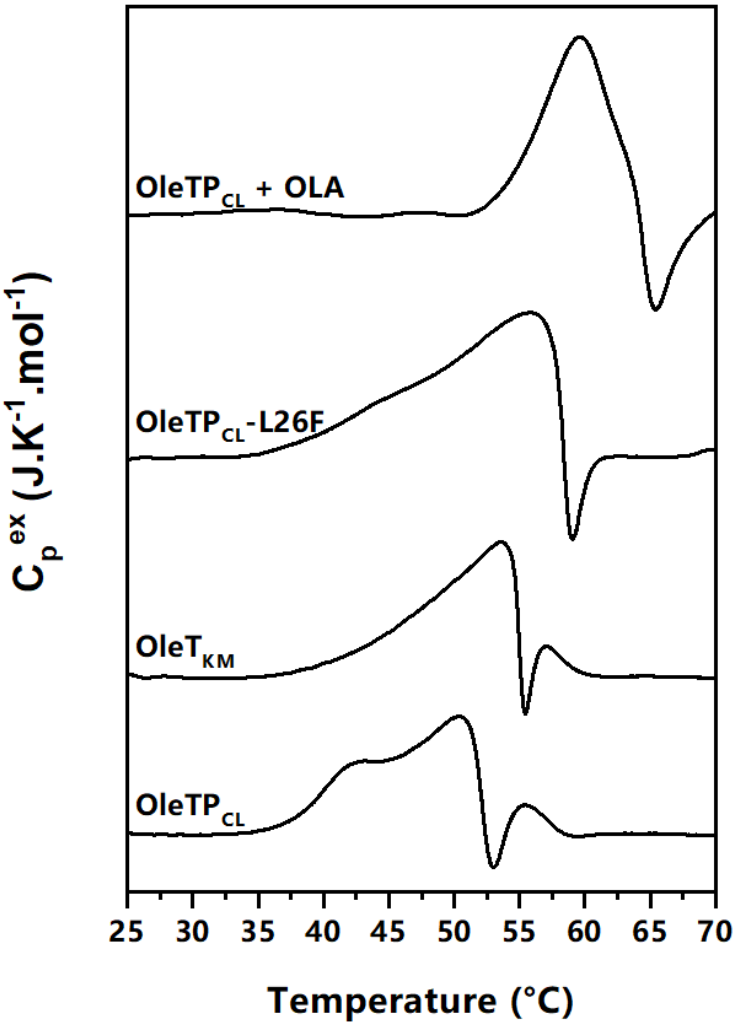

Supplementary Figure 20. Differential scanning calorimetry (DSC) analysis of OleTP$_{CL}$, OleTP$_{CL}$-L26F, and OleT$_{KM}$. All measurements were carried out at a scan rate of 1°C/min, using 100 µM protein in purification buffer [30 mM phosphate buffer, 300 mM NaCl, 5% glycerol, pH 7.5]. Alternatively, OleTP$_{CL}$ was also scanned in the presence of 500 µM oleic acid.

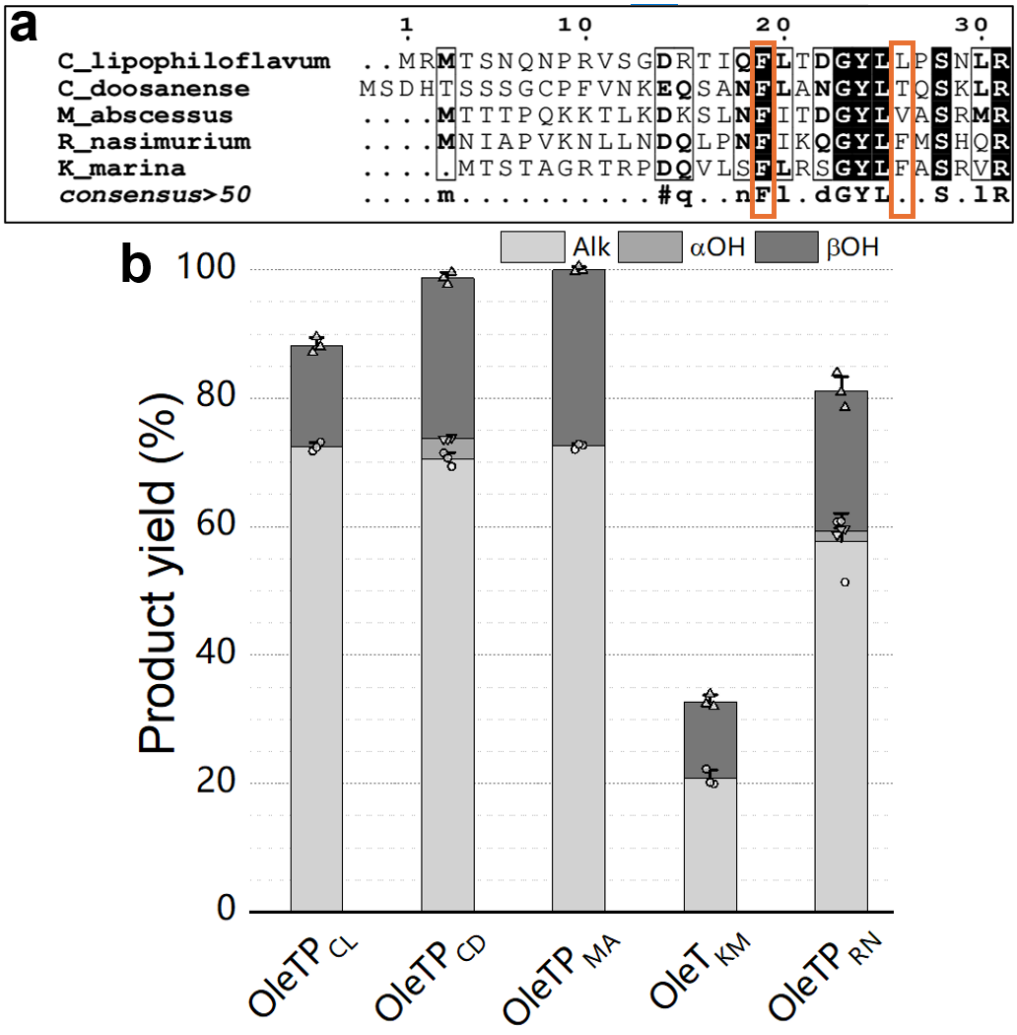

Supplementary Figure 21. (a) Sequence alignment highlighting $OleTP_{CL}$ orthologs possessing conserved F19 and short side-chain residues at position 26. **(b)** Product yield of turnover reactions conducted with $OleTP_{CL}$ orthologs from *Corynebacterium doosanense* and *Mycobacterium abscessus* with oleic acid. Product yield for $OleT_{KM}$ and $OleTP_{RN}$ is displayed to better visualize the higher F19 mobility as a positive feature towards alkene production from oleic acid. Experimental conditions: 2 µM enzyme, 500 µM total substrate, 600 µM H_2O_2 in 100 mM sodium phosphate buffer (pH 7.5) for 1 h. The optimal temperatures previously characterized were employed for enzyme assays: 37°C for $OleTP_{MA}$ and $OleTP_{RN}$, 40°C for $OleT_{KM}$, and 45°C for $OleTP_{CL}$ and $OleTP_{CD}$. Results are expressed as mean ± SD from three independent experiments (n = 3).

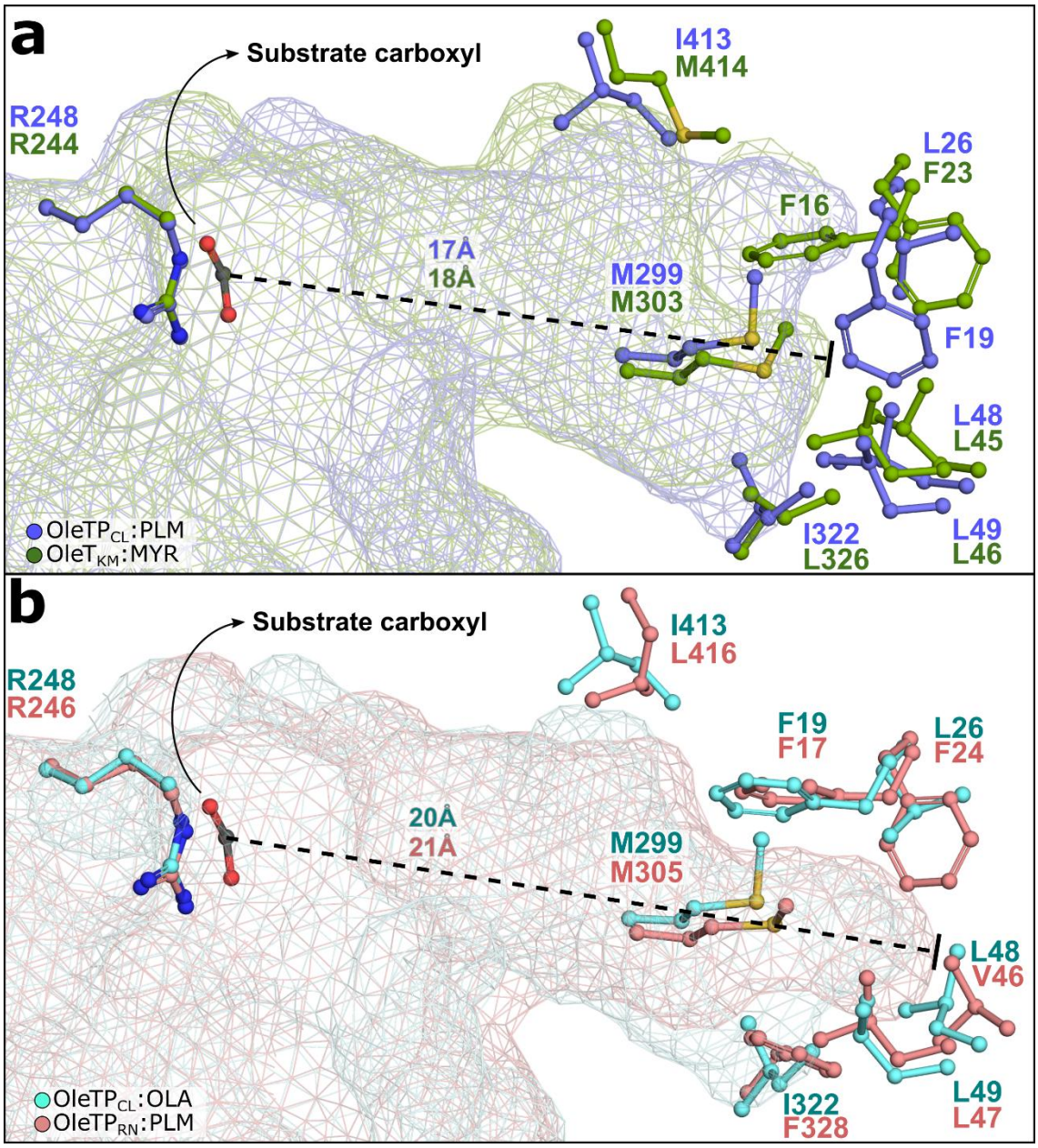

Supplementary Figure 22. Comparison of pocket distal end conformation of OleT$_{KM}$ and OleTP$_{CL}$ complexed with palmitic acid **(a)**, and OleTP$_{RN}$ and OleTP$_{CL}$ complexed with oleic acid **(b)**. The representations highlight important amino acids for binding pocket delimitation and the estimated distance between the substrate carboxyl carbon and pocket distal end. The protein internal surfaces are represented as wire to improve the visualization of both binding pockets.

.

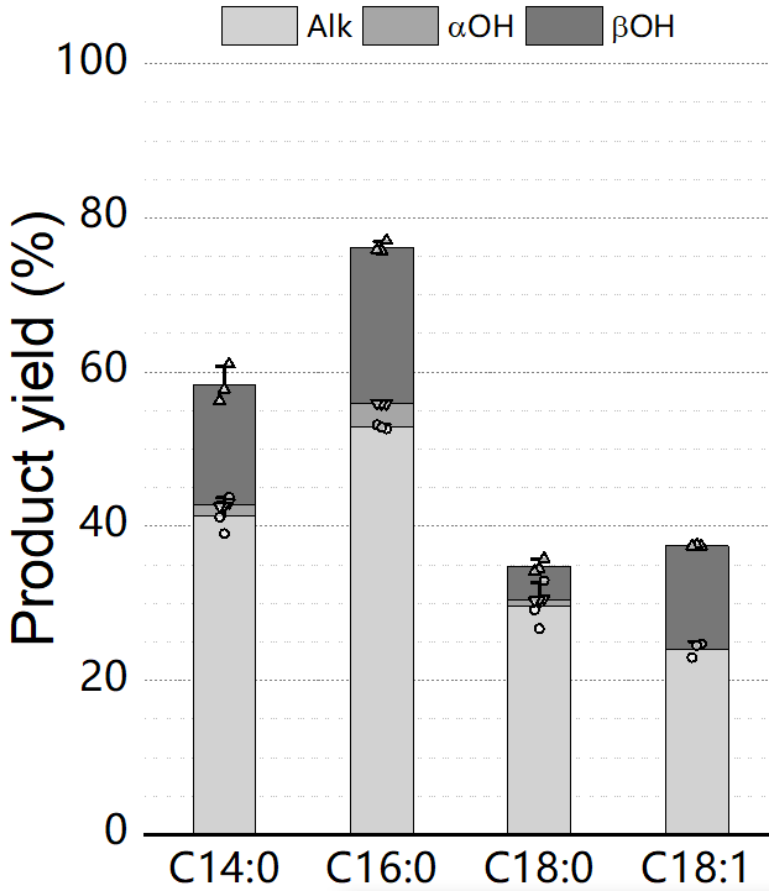

Supplementary Figure 23. The product yield of turnover reactions was conducted with $OleT_{KM}$-L45V using different FA substrates. Experimental conditions: 2 μM enzyme, 500 μM total substrate, 600 μM H_2O_2, at 40°C in 100 mM sodium phosphate buffer (pH 7.5) for 1 h. Results are expressed as mean ± SD from three independent experiments (n = 3).

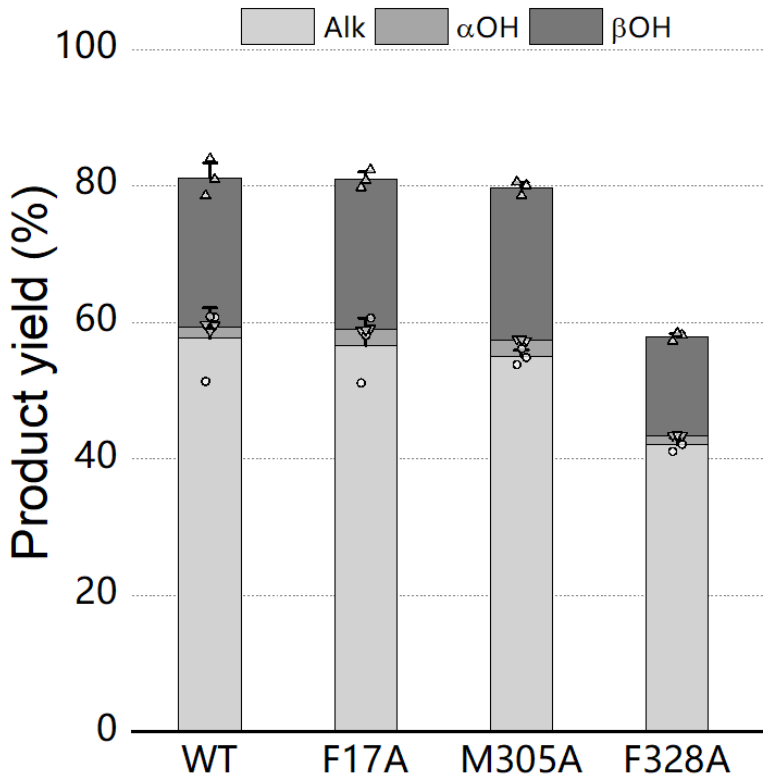

Supplementary Figure 24. The product yield of turnover reactions conducted with $OleTP_{RN}$ WT and their mutants with oleic acid. Experimental conditions: 2 μM enzyme, 500 μM total substrate, 600 μM H_2O_2, 37°C in 100 mM sodium phosphate buffer (pH 7.5) for 1 h. Results are expressed as mean ± SD from three independent experiments (n = 3).

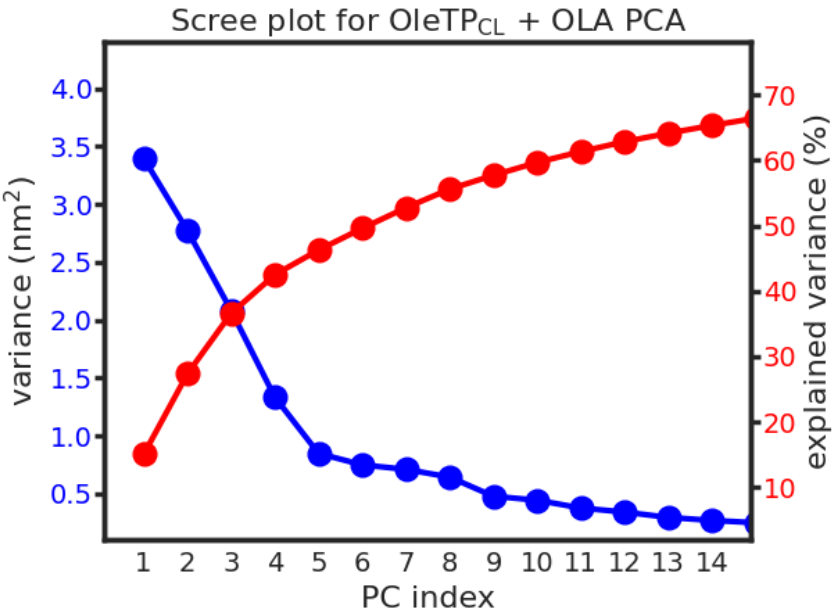

Supplementary Figure 25. Eigenvalues and eigenvectors obtained by principal component analysis of OleTP$_{CL}$ complexed with oleic acid.

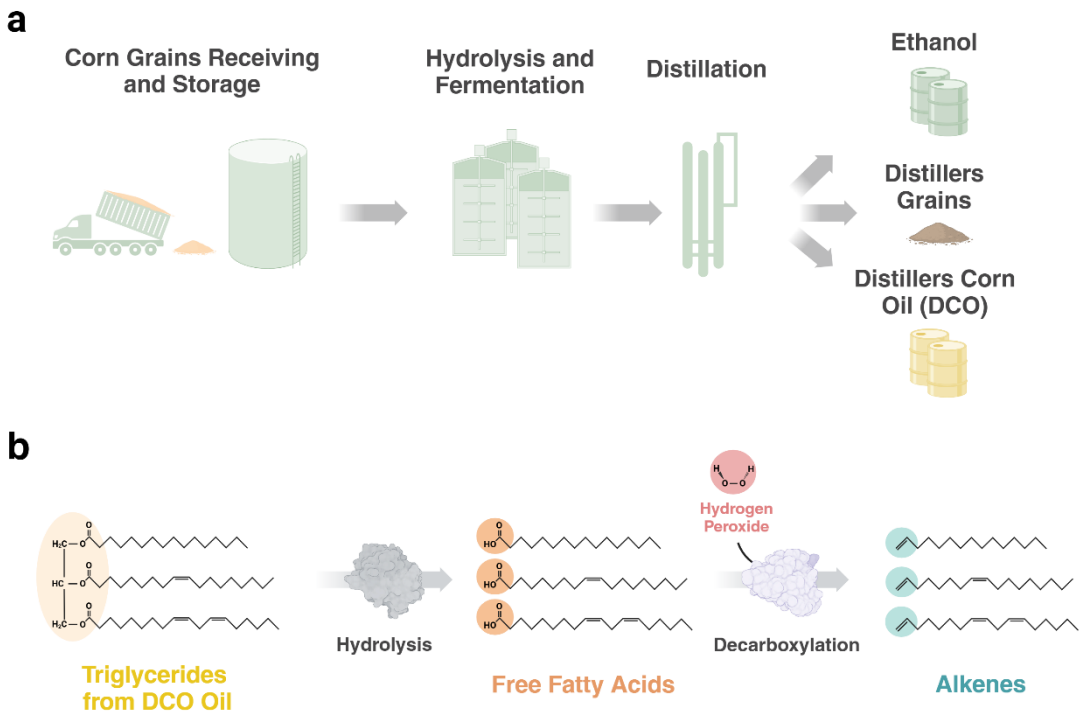

Supplementary Figure 26. Schematic representation of a corn biorefinery and the biosynthesis of alkenes from distilled corn oil (DCO). **(a)** Overview of the production processes for ethanol, DCO, and distillers grains (DG) within a corn biorefinery. **(b)** Biocatalytic pathway for the conversion of DCO oil into renewable alkenes. Created in BioRender. Zanphorlin, L. (2024) https://BioRender.com/t64a706.

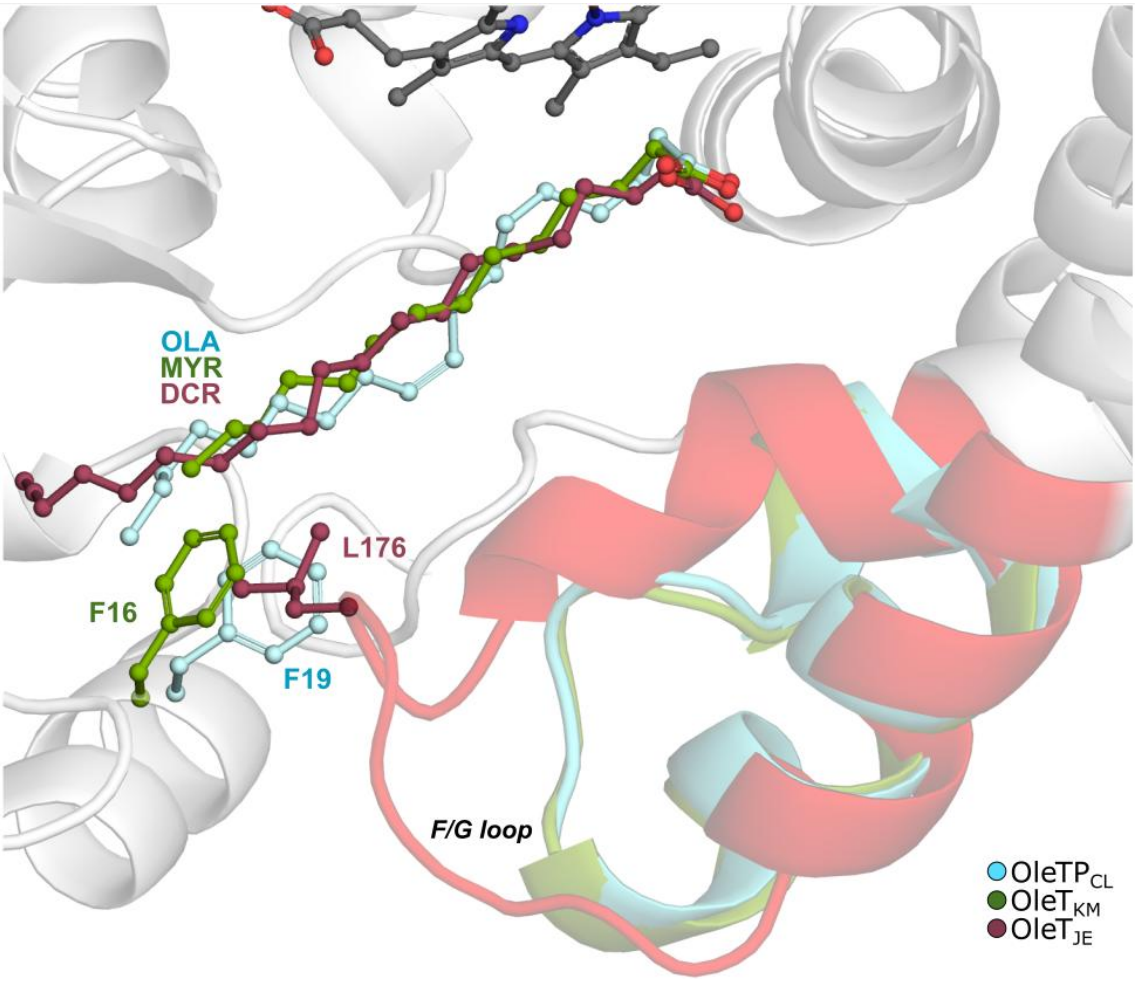

Supplementary Figure 27. Representation demonstrating the single interaction unit responsible for long substrate support, carried out by the long F/G loop in OleT$_{JE}$, while in the short F/G loop members OleTP$_{CL}$ and OleT$_{KM}$, this support is exerted by the loop itself alongside with the hydrophobic cradle, represented by F19.

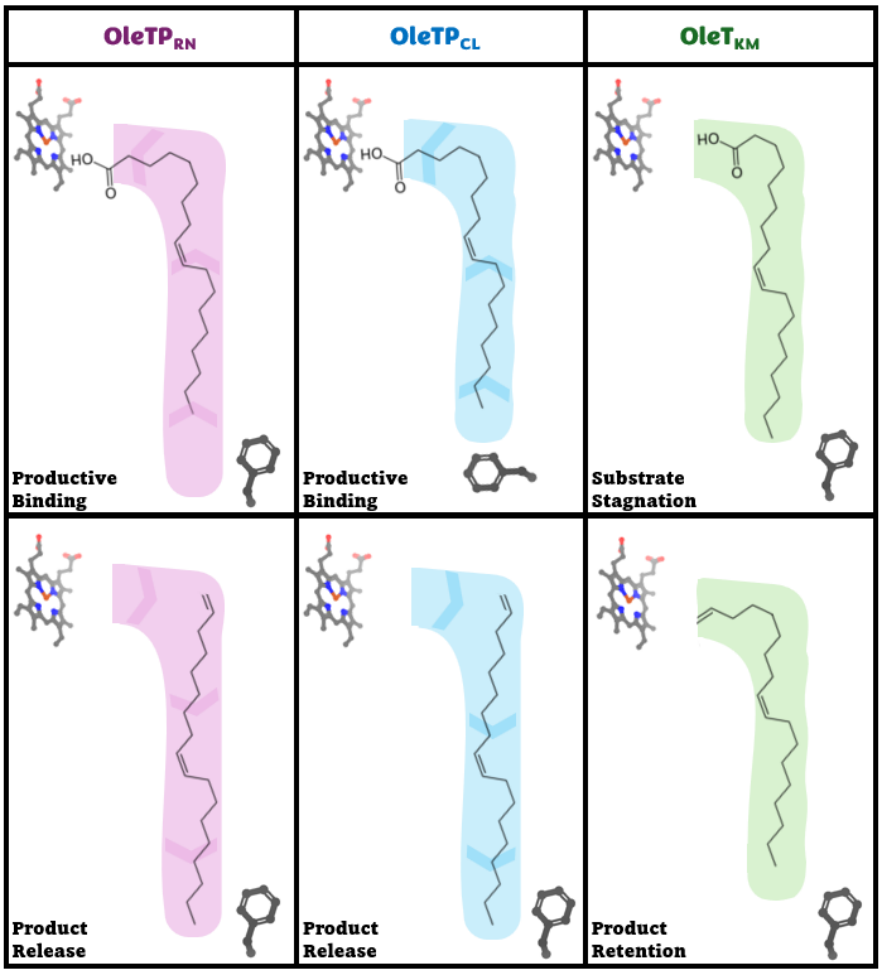

Supplementary Figure 28. Representation of proposed mechanism for oleic acid decarboxylation among characterized Cluster II decarboxylases. In this scheme, OleTP$_{RN}$ and OleTP$_{CL}$ are able to propel substrate Cβ towards the heme group for catalysis and afterward pushing the product backwards to promote its release, while in OleT$_{KM}$, neither substrate can efficiently move on towards heme nor product is freed from the binding pocket, leading to an ineffective oleic acid conversion and thereby enzyme inhibition.

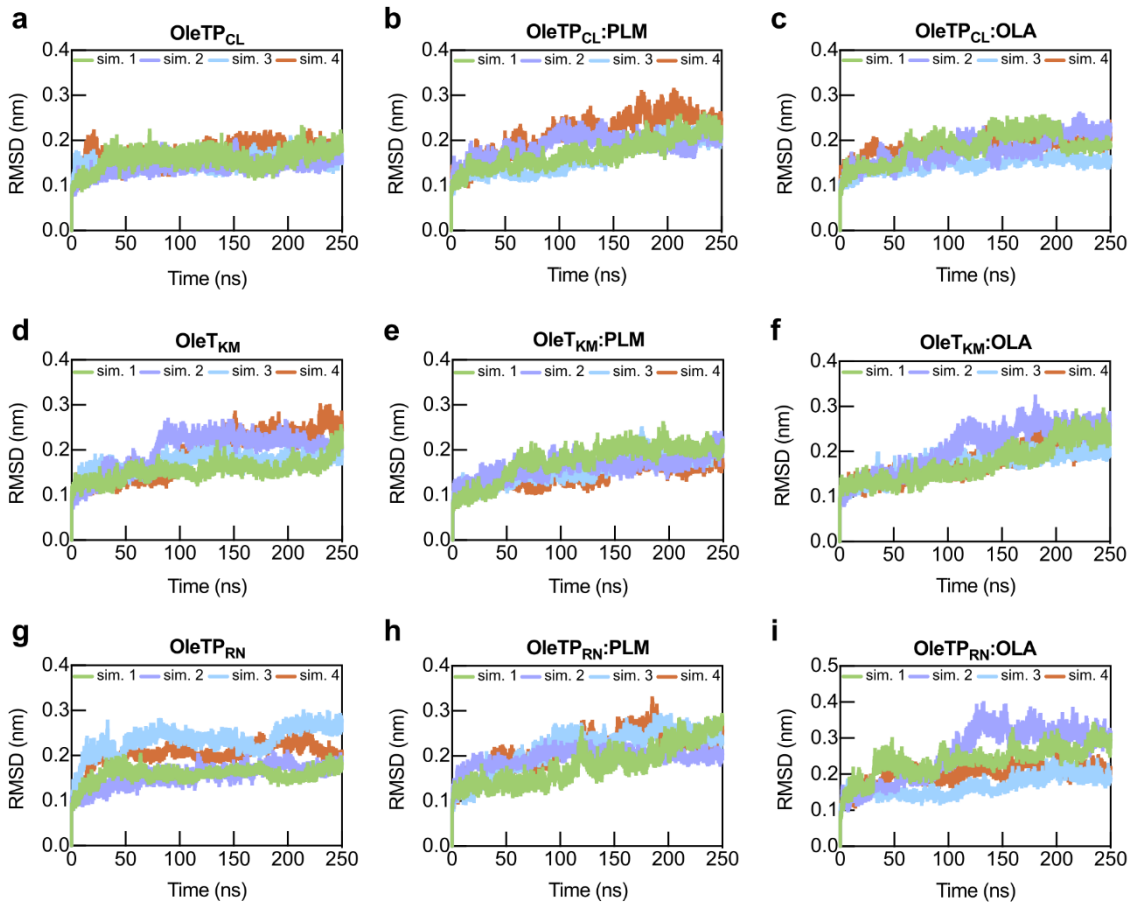

Supplementary Figure 29. Protein backbone RMSD values along the trajectories of 250 ns for four independent simulations (sim.1; sim.2; sim.3 and sim.4) of the systems OleTP$_{CL}$ Phe19 **(a-c);** OleT$_{KM}$ Phe16 **(d-f)** and OleTP$_{RN}$ Phe17 for the protein without substrate and complexed with palmitic (PLM) and oleic acid (OLA), respectively.

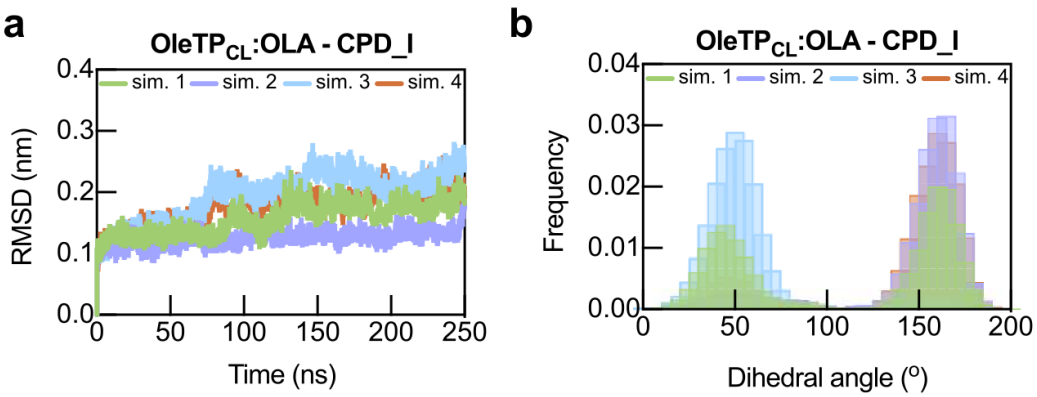

Supplementary Figure 30. Molecular dynamics simulations of OleTP$_{CL}$ considering the CpdI in the presence of oleic acid (OLA). a) RMSD values throughout 250 ns of MD simulations. b) Frequency of the dihedral angles' distribution. Four independent simulations (sim. 1, sim. 2, sim. 3 and sim. 4) were performed. CPDI forcefield parameters from [4].

Supplementary Table 1. Identity matrix (%) of $OleTP_{RN}$ orthologs in *Corynebacterium* and *Kocuria* genera.

		1	**2**	**3**	**4**	**5**	**6**	**7**	**8**	**9**	**10**	**11**	**12**	**13**	**14**	**15**	**16**	**17**	**18**	**19**	**20**	**21**	**22**	**23**	**24**	**25**	**26**	**27**	**28**	**29**
1	$OleTP_{RN}$	-	52	53	51	50	51	54	56	54	55	57	57	56	55	55	47	47	52	28	28	30	54	54	54	53	54	53	35	30
2	*C. mycetoides*		-	83	77	77	69	58	50	47	49	52	55	52	53	51	49	49	51	28	27	27	52	52	52	52	53	52	36	31
3	*C. qintianiae*			-	79	79	73	61	51	47	49	53	54	52	53	52	50	50	51	28	27	28	51	51	53	53	52	51	35	30
4	*C. sanguinis*				-	99	72	58	49	46	48	52	55	51	53	50	50	49	51	30	27	28	51	51	52	52	52	51	35	31
5	*C. lipophiloflavum*					-	71	58	49	46	48	52	55	51	54	50	49	49	51	30	27	28	51	51	52	52	52	51	35	31
6	*C. capitovis*						-	56	49	47	49	55	55	52	54	50	49	48	51	28	26	28	52	52	53	52	52	51	37	27
7	*C. massiliense*							-	52	51	54	57	58	55	61	56	53	52	54	28	28	28	54	54	54	54	54	53	36	28
8	*C. epidermidicanis*								-	63	63	59	57	56	56	55	49	49	50	27	29	30	56	56	58	56	57	57	36	27
9	*C. kalinowskii*									-	62	58	57	57	56	55	46	46	48	25	25	27	54	54	54	52	53	53	35	26
10	*C. incognita*										-	61	57	58	56	55	51	50	51	27	27	29	56	56	58	57	58	57	38	29
11	*C. heidelbergense*											-	60	61	58	60	50	50	50	28	28	29	61	61	61	60	62	61	39	28
12	*C. maris*												-	71	67	65	55	55	58	29	30	31	62	62	61	61	61	60	39	26
13	*C. halotolerans*													-	64	65	54	54	54	28	29	29	63	63	62	61	61	60	38	28
14	*C. pollutisoli*														-	61	53	53	54	30	31	29	60	60	60	60	59	60	40	28
15	*C. occultum*															-	52	52	54	28	29	31	60	60	59	59	58	58	37	29
16	*C. efficiens*																-	98	58	26	28	30	52	52	53	52	54	53	37	27
17	*C. gallinarum*																	-	58	27	28	30	52	52	53	53	53	53	36	27
18	*C. doosanense*																		-	27	26	28	52	52	53	52	54	53	36	28
19	*K. palustris*																			-	57	42	29	29	29	29	28	29	33	32
20	*K. polaris*																				-	42	28	28	29	29	28	28	33	26
21	*K. rosea*																					-	30	30	32	32	31	32	34	33
22	*K. marina*																						-	99	76	76	75	75	41	27
23	*K. indica*																							-	77	76	75	75	41	27
24	*K. salsicia*																								-	99	90	91	41	28
25	*K. varians*																									-	89	91	41	28
26	*K. rhizophila*																										-	93	42	28
27	*K. tytonicola*																											-	41	28
28	*K. flava*																												-	26
29	$OleT_{JE}$																													-

Supplementary Table 2. K_D (μM) of saturated C12-C18 and unsaturated C18:1 fatty acids with $OleTP_{CL}$ and $OleT_{KM}$.

	$OleTP_{CL}$			**$OleT_{KM}$**		
Substrate	**K_d**	**S.D.**	**R^2**	**K_d**	**S.D.**	**R^2**
C12:0	2.82	0.30	0.988	6.79	1.19	0.994
C14:0	2.15	0.17	0.992	7.32	1.34	0.990
C16:0	1.34	0.08	0.995	7.66	1.48	0.988
C18:0	1.76	0.15	0.992	6.63	1.26	0.988
C18:1	1.64	0.11	0.995	6.08	0.93	0.990

Supplementary Table 3. Alkene production (%) among total fatty acid conversion of $OleTP_{CL}$, $OleT_{KM}$, $OleTP_{RN,}$ and their mutants, and $OleTP_{CD}$ and $OleTP_{MA}$. NP = Not performed. (*) = Hydroxy-fatty acids below the detection limit.

	C10:0	**C12:0**	**C14:0**	**C16:0**	**C18:0**	**C20:0**	**C18:1**
$OleTP_{CL}$	100.0*	85.2	67.9	83.1	87.2	71.2	82.1
$OleTP_{CL}$-V86F	NP	NP	69.8	82.7	85.0	NP	82.2
$OleTP_{CL}$-H92Q	NP	NP	39.1	49.2	61.3	NP	64.1
$OleTP_{CL}$-L26F	NP	58.1	74.3	87.5	84.7	NP	64.4
$OleT_{KM}$	100.0*	88.0	84.1	90.8	88.9	81.1	87.1
$OleT_{KM}$-F16A	NP	NP	NP	NP	NP	NP	59.8
$OleT_{KM}$-M303A	NP	NP	NP	NP	NP	NP	63.9
$OleT_{KM}$-L45V	NP	NP	70.8	69.4	85.1	NP	64.3
$OleT_{KM}$-L326F	NP	NP	NP	NP	NP	NP	60.1
$OleT_{KM}$-M414L	NP	NP	NP	NP	NP	NP	71.1
$OleTP_{RN}$	NP	NP	NP	NP	NP	NP	71.4
$OleTP_{RN}$-F17A	NP	NP	NP	NP	NP	NP	69.9
$OleTP_{RN}$-M305A	NP	NP	NP	NP	NP	NP	68.2
$OleTP_{RN}$-F328A	NP	NP	NP	NP	NP	NP	72.8
$OleTP_{CD}$	NP	NP	NP	NP	NP	NP	71.1
$OleTP_{MA}$	NP	NP	NP	NP	NP	NP	72.5

Supplementary Table 4. Data collection and refinement statistics for crystallographic data. Values in parentheses represent the higher-resolution shell.

	OleTP$_{CL}$-C16	**OleTP$_{CL}$-C18:1**	**OleT$_{KM}$-C14**
Data collection			
Wavelength (Å)	0.977180	0.977180	0.977180
Detector	Dectris Pilatus 2M	Dectris Pilatus 2M	Dectris Pilatus 2M
Temperature (K)	100	100	100
Resolution range (Å)	49.74 – 1.80	48.95 - 1.70	46.79 - 2.05
Space group	$C222_1$	$C222_1$	$P3_121$
Cell dimensions			
a, *b*, *c* (Å)	157.93, 171.02, 122.31	158.91, 170.37, 121.60	88.72, 88.72, 117.98
A, β, γ (°)	90, 90, 90	90, 90, 90	90, 90, 120
Unique reflections	152317 (24,408)	179,979 (28,868)	34,276 (5,461)
Multiplicity	13.53 (13.59)	13.55 (13.78)	20.05 (19.54)
Completeness (%)	100.0 (100.0)	100.0 (100.0)	100.0 (100.0)
Mean *I* / σI	9.12 (1.01)	9.27 (0.93)	18.07 (0.94)
R-meas	0.316 (2.792)	0.233 (2.833)	0.100 (3.046)
$Cc_{1/2}$ (%)	99.6 (46.9)	99.8 (41.6)	100.0 (45.5)
Refinement			
R-work	0.179 (0.443)	0.169 (0.469)	0.202 (0.340)
R-free	0.213 (0.455)	0.197 (0.483)	0.227 (0.360)
No. Atoms	10793	10832	3592
Protein	9703	9727	3334
Ligand/Ion	183	189	95
Water	907	916	163
B-factors			
Protein	30.75	29.23	59.9
Ligand/ion	27.17	26.30	64.0
Water	37.43	37.51	61.3
R.M.S. Deviations			
Bond lengths (Å)	0.44	0.56	0.26
Bond angles (°)	0.62	0.69	0.53
Ramachandran analysis			
Favored (%)	98.4	98.0	97.0
Allowed (%)	1.2	1.3	2.8
Outliers (%)	0.4	0.4	0.2

Supplementary Table 5. The fatty acid profile found in distillers corn oil (DCO).

Fatty acids	DCO oil [1, 2, 3]
Caprylic acid (C8:0)	< 0.10 %
Capric acid (C10:0)	< 0.10 %
Lauric acid (C12:0)	0.11 ± 0.01 %
Myristic acid (C14:0)	0.11 ± 0.01 %
Palmitic acid (C16:0)	14.80 ± 0.10 %
Palmitoleic (16:1)	0.10 ± 0.01 %
Stearic acid (C18:0)	2.00 ± 0.10 %
Oleic acid (C18:1)	32.40 ± 0.10 %
Linoleic acid (C18:2)	48.70 ± 0.10 %
Linolenic acid (C18:3)	1.20 ± 0.10 %
Arachidic acid (C20:0)	0.37 ± 0.01 %
Behenic acid (C22:0)	0.12 ± 0.01 %
Erucic acid (C22:1)	< 0.10 %
Lignoceric acid (24:0)	0.11 ± 0.01 %
Acid value (mg KOH/g)	11.69 ± 0.11

[1] %A = The percentage of the normalized area indicates the relative distribution of each compound identified in the oil sample. The equipment applied was a gas chromatograph with a flame ionization detector - Shimadzu GC2010.

[2] The mean and standard deviation results were obtained from two DCO oil samples.

[3] The acidity, or Free Fatty Acid (FFA) content, was determined using a volumetric titration method. In this method, the sample was dissolved in a mixture of ether: ethanol (2:1, v/v), followed by titration with 0.1 mol/L KOH solution using 0.032 mol/L phenolphthalein.

Supplementary Table 6. Factor levels and experimental parameters used in the Plackett-Burman (PB) design.

Variables	Units	-1	0	1
$OleTP_{CL}$	µM	0.50	2.75	5.00
Commercial lipase from *Aspergillus oryzae*	mg/mL	0.12	0.62	1.12
Triton X-100	%	0.0	0.5	1.0
H_2O_2	mM	16	26	36
Agitation	rpm	400	600	800

Supplementary Table 7. Data from the Plackett-Burman (PB) design, showing actual values and coded levels (in parentheses).

(0.5-mL reaction system)								
Runs	**OleTP$_{CL}$ (µM)**	**Lipase (mg/mL)**	**Triton (%)**	**H_2O_2 (mM)**	**Agitation (rpm)**	**Total alkenes (µM)**	**Total alkenes (g/L)**	**TTN**
PB1	5.00 (1)	0.12 (-1)	1.0 (1)	16 (-1)	400 (-1)	3518.483 ± 137.091	0.811 ± 0.032	703.697 ± 27.418
PB2	**5.00 (1)**	**1.12 (1)**	**0.0 (-1)**	**36 (1)**	**400 (-1)**	**6813.350 ± 398.717**	**1.570 ± 0.092**	**1362.670 ± 79.743**
PB3	0.50 (-1)	1.12 (1)	1.0 (1)	16 (-1)	800 (1)	1878.303 ± 103.915	0.435 ± 0.024	3756.607 ± 207.830
PB4	5.00 (1)	0.12 (-1)	1.0 (1)	36 (1)	400 (-1)	4494.780 ± 206.002	1.038 ± 0.048	898.956 ± 41.200
PB5	5.00 (1)	1.12 (1)	0.0 (-1)	36 (1)	800 (1)	6136.567 ± 477.821	1.420 ± 0.111	1227.313 ± 95.564
PB6	5.00 (1)	1.12 (1)	1.0 (1)	16 (-1)	800 (1)	3393.783 ± 145.668	0.782 ± 0.034	678.757 ± 29.134
PB7	0.50 (-1)	1.12 (1)	1.0 (1)	36 (1)	400 (-1)	1787.333 ± 86.753	0.414 ± 0.020	3574.667 ± 173.506
PB8	0.50 (-1)	0.12 (-1)	1.0 (1)	36 (1)	800 (1)	1510.993 ± 31.532	0.348 ± 0.007	3021.987 ± 63.063
PB9	0.50 (-1)	0.12 (-1)	0.0 (-1)	36 (1)	800 (1)	1210.483 ± 31.826	0.280 ± 0.007	2420.967 ± 63.651
PB10	5.00 (1)	0.12 (-1)	0.0 (-1)	16 (-1)	800 (1)	1524.093 ± 2.837	0.353 ± 0.001	304.819 ± 0.567
PB11	0.50 (-1)	1.12 (1)	0.0 (-1)	16 (-1)	400 (-1)	3218.110 ± 46.943	0.745 ± 0.011	6436.220 ± 93.886
PB12	0.50 (-1)	0.12 (-1)	0.0 (-1)	16 (-1)	400 (-1)	1324.663 ± 16.663	0.307 ± 0.004	2649.327 ± 33.326
PB13	2.75 (0)	0.62 (0)	0.5 (0)	26 (0)	600 (0)	5973.860	1.382	2172.313
PB14	2.75 (0)	0.62 (0)	0.5 (0)	26 (0)	600 (0)	5837.250	1.350	2122.636
PB15	2.75 (0)	0.62 (0)	0.5 (0)	26 (0)	600 (0)	5647.490	1.306	2053.633
PB16	2.75 (0)	0.62 (0)	0.5 (0)	26 (0)	600 (0)	6130.370	1.418	2229.225

(50-mL reaction system)								
	OleTP$_{CL}$ (µM)	**Lipase (mg/mL)**	**Triton (%)**	**H_2O_2 (mM)**	**Agitation (rpm)**	**Total alkenes (µM)**	**Total alkenes (g/L)**	**TTN**
	5.00	**1.12**	**0.0**	**36**	**400**	**7352.983 ± 257.379**	**1.703 ± 0.060**	**1470.597 ± 51.476**

Supplementary Table 8. Alkene production by a cell-free system containing P450 decarboxylases.

System	Alkene titer	Feedstock	Reference
Lipase from *Thermomyces lanuginosus*/ $OleT_{JE}$	0.07 g/L	Soybean oil	[1]
Cellulose/ Dockerin/ $OleT_{JE}$/ lipase from *Thermomyces lanuginosus*	0.2 g/L	Cooking oil	[2]
Lipase from *Candida rugose*/ $OleT_{JE}$/ AldO from *Streptomyces coelicolor*	0.53 g/L (in 0.2-mL reaction system)	Coconut oil	[3]
Lipase from *Candida rugose*/ $OleT_{JE}$/ AldO from *Streptomyces coelicolor*	0.49 g/L (in 10-mL reaction system)	Coconut oil	[3]
Lipase from *Aspergillus oryzae*/ $OleTP_{CL}$	1.57 g/L (in 0.5-mL reaction system)	Distillers corn oil	This work
Lipase from *Aspergillus oryzae*/ $OleTP_{CL}$	1.70 g/L (in 50-mL reaction system)	Distillers corn oil	This work

Supplementary Table 9. List of primers employed for site-directed mutagenesis.

Primer name	Sequence (5' - 3')
$OleTP_{CL}$-V86F_Fw	CGCGCTGTTTGGTAAAGGCGCGGTTCAC
$OleTP_{CL}$-V86F_Rv	TTACCAAACAGCGCGTCACCAATAACTG
$OleTP_{CL}$-H92Q_Fw	CGGTTCAGAACCTGGATGGCGAG
$OleTP_{CL}$-H92Q_Rv	CCAGGTTCTGAACCGCGCCTTTAC
$OleTP_{CL}$-L26F_Fw	TACCTGTTTCCGAGCAACCTGCGTAAG
$OleTP_{CL}$-L26F_Rv	GCTCGGAAACAGGTAACCATCGGTC
$OleT_{KM}$-F16A_Fw	TTCTGAGCGCCCTGCGTAGCGGCTACCTG
$OleT_{KM}$-F16A_Rv	ACGCAGGGCGCTCAGAACCTGGTCCG
$OleT_{KM}$-M303A_Fw	TCGTTCCGGCGCTGCCGGCGG
$OleT_{KM}$-M303A_Rv	AGCGCCGGAACGAACGGATAAACACGACGCAC
$OleT_{KM}$-L45V_Fw	CATGAACGTGCTGGGCAAGCGTAGC
$OleT_{KM}$-L45V_Rv	CCCAGCACGTTCATGCTAACCGGCGC
$OleT_{KM}$-L326F_Fw	GCGTGTTTTCATCGACATTCTGGGTACCAACAACGATCCGGC
$OleT_{KM}$-L326F_Rv	ATGTCGATGAAAACACGCTGGCCTTTGTGAATCGGGC
$OleT_{KM}$-M414L_Fw	TGGACCCACTTGCTGACCCGTCCGGC
$OleT_{KM}$-M414L_Rv	TCAGCAAGTGGGTCCAGCTAAAGGTCAGATCGTCCGG

Supplementary Methods

Substrate binding (fatty acids) titrations and determination of dissociation constants

The substrate-binding titrations were performed with $OleTP_{CL}$ and $OleT_{KM}$ against saturated fatty acids (C12 to C18), and an unsaturated fatty acid (C18:1). The fatty acids stocks (10 mM) were prepared in ethanol and Triton X100 solution (70/30 v/v). The titrations were performed by gradual additions of fatty acids into a cuvette containing 1 mL of 5 µM of the enzyme [reaction buffer: 100 mM potassium phosphate (pH 7.5), 100 mM NaCl, and 5 % (v/v) glycerol]. A spectrum was collected after each addition of fatty acid aliquot (300-750 nm spectral range), and the changes in the absorption (ΔA), induced by substrate binding, were calculated by the difference between the absorbance maxima and minima at 422 nm (LS) and 399 nm (HS). ΔA at 399 and 422 nm were added together (ΔAmax) and were plotted as a function of the total concentration of the substrate for dissociation constant (KD) determination by Morrison's quadratic equation fitting.

Ferrous oxidation xylenol-orange (FOX) assays

To investigate the optimum reaction conditions of the enzymes, ferrous oxidation xylenol-orange (FOX) assays were performed, allowing the identification of peroxide oxidation in the reaction. The reactions were carried out in 96-well plates, with a reaction volume of 100 µL composed of 0.5 µM enzyme and 200 µM palmitic acid (prepared in pure ethanol) diluted in reaction buffer [100 mM sodium phosphate, pH 7.5]. The reaction was incubated for 5 min at 37°C, then 100 µM of hydrogen peroxide was added, and the system was incubated again for 10 min at 37°C (Veriti Thermal Cycler - Applied Biosystems, Waltham, USA). After this period, the reactions were quenched by temperature increasing to 70 °C for 5 min. Then, 25 µL of the reaction mixture was added to 75 µL water and 100 µL of FOX solution (0.25 mM xylenol orange, 0.25 mM Fe_2SO_4, 50 mM H_2SO_4, and 3% ethanol). Posteriorly, the samples were incubated at 60 °C for 5 min, and 100 µL was used for the final absorbance measured at 560 nm using an Infinite 200 PRO microplate reader (TECAN Group Ltd., Mannedorf, CHE). The negative controls were performed without substrate. The optimum pH varied from 4 to 10, using the following buffers: sodium-citrate (pH 4.0, 4.5, 5.0, and 5.5), sodium phosphate (pH 6.0, 6.5, 7.0, and 8.0), Tris-HCl (pH 9.0), and glycine (pH 10.0). The influence of

temperature was evaluated by incubating the reaction in a range from 20 to 60°C. The concentration of NaCl and KCl were evaluated from 0 to 500 mM. The measurements were expressed as relative activity (%), considering the maximum catalytic activity observed for the best reactional condition. Experiments were carried out in quadruplicate.

SEC-MALS analysis

Size-exclusion chromatography coupled with multi-angle light scattering (SEC-MALS) experiments were performed at 25 °C using an eight-angle static light scattering detector DAWN8 and Optilab® refractive index monitor (Wyatt Technology, Santa Barbara, USA) coupled to an Agilent HPLC 1260 Infinity II system with a Superdex® 200 Increase 10/300 GL analytical size-exclusion column (GE Healthcare). 200 µL from purified enzyme at 50 µM was injected into the column and eluted in GF buffer (30 mM sodium phosphate, 500 mM NaCl, 5% w/v glycerol, pH 7.5).

Circular Dichroism Analysis

Far-UV circular dichroism (CD) spectra were taken on a JASCO J-815 CD spectrometer controlled by a CDF-426S Peltier temperature control system (Jasco Analytical Instruments, Oklahoma, EUA). CD spectra were measured with 0.3 mg/mL of each enzyme separately (wild-type and mutants) in buffer [150 mM NaCl, 100 mM sodium phosphate, 5 % w/v glycerol, pH 7.5] at 20 °C. A quartz cuvette with a 1-mm path length was used for all CD experiments. Each spectrum was an average of ten scans, measured from 190 to 260 nm, with a bandwidth of 2.0 nm and a response time of 4 s. Thermal unfolding experiments were determined by measuring the CD signal at 222 nm with increasing temperature in a continuous ramp mode of 20 to 100 °C, at 1 °C min^{-1}. The observed ellipticity (θ degree-1) was normalized against the protein concentration and reported as the mean residue molar ellipticity (θ degree-1 cm2 dmol-1). The melting temperature (Tm) was determined according to Boltzmann sigmoidal fitting of the data obtained in the CD denaturation curve.

Enzyme thermal resistance

Protein thermal resistance was performed at constant incubation at 42°C in a SPARK microplate reader (TECAN Group Ltd., Mannedorf, CHE). For this, 100 µL enzyme solution was incubated in a 384-well plate and monitored by absorbance at 350 nm for 40 hours at 30 min increments. 350 nm corresponds to the maxima absorbance of

the free heme group, which was released after protein denaturation. Enzymes at 10 μM solution in 30 mM phosphate buffer (pH 7.5), 300 mM NaCl, and 5% glycerol were employed with and without the addition of 500 μM substrate (C14:0 or C18:1). In order to avoid sample concentration by evaporation, a humidifying chamber was employed. Samples were assayed in quadruplicate using a buffer as a blank control.

Differential Scanning Calorimetry (DSC)

Calorimetric experiments were performed to address the thermal stability of $OleTP_{CL}$ and $OleT_{KM}$ (and mutants) using a VP-DSC device (Microcal, GE Healthcare, Northampton, USA). For this, 100 μM protein in 30 mM phosphate buffer (pH 7.5), 300 mM NaCl, and 5% glycerol were scanned at a rate of 1 °C/min over the range of 15-90 °C at 0.5 °C increments. The DSC profile was buffer subtracted, concentration normalized, and the resultant endotherms integrated following the assignment of pre- and post-transition baselines. As thermal-induced unfolding of P450 is irreversible due to heme group detachment, only heating conditions were tested, focusing on the values of transition temperatures (Tm). For denaturation curve of $OleTP_{CL}$ with oleic acid, 500 μM substrate was employed using buffer subtraction also performed with the substrate.

Supplementary References

1. Yan, J., Liu, Y., Wang, C., Han, B. & Li, S. Assembly of lipase and P450 fatty acid decarboxylase to constitute a novel biosynthetic pathway for production of 1-alkenes from renewable triacylglycerols and oils. *Biotechnol Biofuels* **8**, 1–10 (2015).

2. Li, F. *et al.* A genetically-encoded synthetic self-assembled multienzyme complex of lipase and P450 fatty acid decarboxylase for efficient bioproduction of fatty alkenes. *Bioresour Technol* **272**, 451–457 (2019).

3. Jiang, Y. *et al.* Establishing an enzyme cascade for one-pot production of α-olefins from low-cost triglycerides and oils without exogenous H2O2 addition. *Biotechnol Biofuels* **13**, 1–11 (2020).

4. Bathelt, C. M., Zurek, J., Mulholland, A. J. & Harvey, J. N. Electronic structure of compound I in human isoforms of cytochrome P450 from QM/MM modeling. *J Am Chem Soc* **127**, (2005).